Across and along-strike crustal structure variations of the western Afar margin and adjacent plateau: Insights from receiver functions analysis

Abdulhakim Ahmed, Cecile Doubre, Sylvie Leroy, Derek Keir, Carolina Pagli, James O. S. Hammond, Atalay Ayele, Maxime Be de Berc, Marc Grunberg, Jerome Vergne, et al.

Journal of African Earth Sciences

Across and along-strike crustal structure variations of the western Afar margin and adjacent plateau: Insights from receiver functions analysis

--Manuscript Draft--

Manuscript Number:	
Article Type:	Research Paper
Keywords:	Africa; Continental margin; Afar margin; Southern Red Sea Rift; Receiver Functions; Crustal Structure
Corresponding Author:	Abdulhakim Ahmed, Ph.D. IPGS Haguenau, Bas-Rhin FRANCE
First Author:	Abdulhakim Ahmed, Ph.D.
Order of Authors:	Abdulhakim Ahmed, Ph.D.
	Cecile Doubre, Dr
	Sylvie Leroy, Dr
	Derek Keir, Dr
	Carolina Pagli, Dr
	James O. S. Hammond, Dr
	Atalay Ayele, Dr
	Maxime Be de Berc
	Mark Grunberg, Dr
	Jerome Vergne, Dr
	Romain Pestourie
	Daniel Mamo
	Birhanu Kibret
	Nadaya Cubas, Dr
	Aude Lavayssière
	Marianne Janowski
	Olivier Lengliné
	Alessandro La Rosa, Dr
	Emma L. Chambers, Dr
	Finnigan Illsley-Kemp, Dr
Abstract:	We used teleseismic receiver function analysis to image the crustal structure beneath 24 broadband seismic stations densely deployed along two profiles traversing different structural units across the western Afar margin. Our high-resolution receiver function results image pronounced spatial variations in the crustal structure along the profiles and provide improved insights to understand how strain is partitioned in the crust during rifting. Beneath the western plateau next to northern Afar, the crust is likely felsic-to-intermediate in composition (average Vp/Vs 1.74), with a step like thinning of the crust from an average of 38 km beneath the western plateau to an average of 22 km beneath the marginal graben. Consistently thicker crust is observed beneath the southern profile (central Afar), showing four distinct regions of uniform crustal thickness: 1) an average crustal thickness of 42 km beneath the western plateau; 2) 34 km beneath the foothills area; 3) 28 km beneath the marginal graben and the wide extensional basin and 4) 21 km beneath the central rift axis. We use crustal thickness results to estimate a stretching factor β of 2.2 and 2.7 for central Afar and northern Afar

	respectively. Our estimated values are lower than $\beta > 3.0$ predicted from plate reconstructions, and we interpret that the variations are best explained by 2-5 km magmatic addition at the base of the crust. The crustal composition beneath the southern profile is more complex with elevated Vp/Vs ratios ranging between 1.79 to 1.85 beneath the western plateau and marginal graben. This is consistent with a greater mafic component and best explained by crust altered by intrusions due to significant pre and syn-rift magmatic activity. Abnormally high Vp/Vs ratios more than 1.90 are observed beneath the axial rift zone of central Afar, which most likely suggesting the localization of partial melt within the crust.

Across and along-strike crustal structure variations of the western Afar margin and adjacent plateau: Insights from receiver functions analysis

Abdulhakim Ahmed[1,2,*], Cecile Doubre[1], Sylvie Leroy[2], Derek Keir[3,4], Carolina Pagli[5,6], James O. S. Hammond[7], Atalay Ayele[8], Maxime Be de Berc[1], Marc Grunberg[9], Jerome Vergne[1], Romain Pestourie[1], Daniel Mamo[8], Birhanu Kibret[8], Nadaya Cubas[2], Aude Lavayssière[10], Marianne Janowski[2], Olivier Lengliné[1], Alessandro La Rosa[4,6], Emma L. Chambers[3,11], Finnigan Illsley-Kemp[12]

[1] *Université de Strasbourg, CNRS, IPGS-UMR 7516, F-67000 Strasbourg, France.*
[2] *Sorbonne Université, CNRS-INSU, Institut des Sciences de la Terre de Paris, ISTEP, Paris, France.*
[3] *School of Ocean and Earth Science, University of Southampton, Southampton, United Kingdom.*
[4] *Dipartimento di Scienze della Terra, Università degli Studi di Firenze, Florence, Italy.*
[5] *School of Earth and Environment, University of Leeds, Leeds, UK.*
[6] *Dipartimento di Scienze della Terra, Università di Pisa, Pisa, Italy.*
[7] *Department of Earth and planetary Sciences, BirkBeck, University of London, Malet Street, London, WC1E 7HX.*
[8] *Institute of Geophysics, Space Science and Astronomy, Addis Ababa University, Addis Ababa, Ethiopia.*
[9] *Université de Strasbourg, CNRS, EOST UMS 830, F-67000 Strasbourg, France.*
[10] *Institut de Physique du Globe de Paris, Sorbonne Paris Cité, Université*
[11] *Dublin Institute for Advanced studies DIAS, Dublin 2, Ireland.*
[12] *School of Geography, Environment and Earth Sciences, University of Wellington, Wellington, New Zealand.*

[*] ***Corresponding Author: Tel: +33618639873 ; email:*** *hakim.qubati66@gmail.com*

Abstract

We used teleseismic receiver function analysis to image the crustal structure beneath 24 broadband seismic stations densely deployed along two profiles traversing different structural units across the western Afar margin. Our high-resolution receiver function results image pronounced spatial variations in the crustal structure along the profiles and provide improved insights to understand how strain is partitioned in the crust during rifting. Beneath the western plateau next to northern Afar, the crust is likely felsic-to-intermediate in composition (average Vp/Vs 1.74), with a step like thinning of the crust from an average of 38 km beneath the western plateau to an average of 22 km beneath the marginal graben. Consistently thicker crust is observed beneath the southern profile (central Afar), showing four distinct regions of uniform crustal thickness: 1) an average crustal thickness of 42 km beneath the western plateau; 2) 34 km beneath the foothills area; 3) 28 km beneath the marginal graben and the wide extensional basin and 4) 21 km beneath the central rift axis. We use crustal thickness results to estimate a stretching

factor β of 2.2 and 2.7 for central Afar and northern Afar respectively. Our estimated values are lower than β > 3.0 predicted from plate reconstructions, and we interpret that the variations are best explained by 2-5 km magmatic addition at the base of the crust. The crustal composition beneath the southern profile is more complex with elevated Vp/Vs ratios ranging between 1.79 to 1.85 beneath the western plateau and marginal graben. This is consistent with a greater mafic component and best explained by crust altered by intrusions due to significant pre and syn-rift magmatic activity. Abnormally high Vp/Vs ratios more than 1.90 are observed beneath the axial rift zone of central Afar, which most likely suggesting the localization of partial melt within the crust.

Keywords: Africa; Continental margin; Afar margin; Southern Red Sea Rift; Receiver Functions; Crustal Structure

1. Introduction

The Afar Depression lies in northeast Africa where the Red Sea and Gulf of Aden oceanic spreading ridges and the intra-continental East-African Rift meet, forming a rift-rift-rift triple junction between the Nubian, Somalian, and Arabian plates (McKenzie et al., 1972; Courtillot, 1982; Tesfaye et al., 2003; Doubre et al., 2017). The Afar Depression is bound by the continental Danakil block to the northeast (Fig. 1), and by the western and southern plateaus, to the west and south respectively. The Afar Depression is thought to have formed shortly after the impact of the Afar mantle plume and associated eruption of the bimodal Ethiopia-Yemen Trap Series of basalts and rhyolitic lavas (Hofmann et al., 1997; Pik et al., 1998, 1999; Pik, 2011). The extension of the proto-African lithosphere started in the Oligo-Miocene (~29-26 Ma) shortly after the peak in Trap Series volcanism at ~29-31 Ma (Wolfenden et al., 2004, 2005; Stab et al., 2016). In the present-day, several magmatic segments are the locus of extensional deformation with networks of normal faults formed above narrow zones of episodic dike intrusion (Fig. 1; Wright et al., 2006; Grandin et al., 2009; Smittarello et al., 2016; Barnie et al., 2016). Therefore, the continental margin of the Afar region is a unique location where the transition from the stable continental plateaus to incipient seafloor spreading within the Afar rift axis is subaerially exposed (Barberi and Varet, 1977;

Hayward and Ebinger, 1996; Beyene and Abdulsalam, 2005; Medynski et al., 2016).

Despite reasonable consensus regarding the locus and mode of upper crustal extension both at the stage of rift initiation and at the present day, few data allow an informed interpretation of the structural evolution of the rifting between these two periods. Continental margins underwater have been intensely investigated to constrain the mechanisms leading to the continental break-up (e.g. Leroy et al., 2012). Particularly, seismic experiments help to draw the geometry of the margin units and quantify, in terms of finite deformation, amount of stretching and thinning due to tectonic processes and also the role of magmatism (e.g. Leroy et al., 2010; Clark et al., 2006; d'Acremont et al., 2005, 2006). However, due to the subaerial exposure, passive seismic experiments and geological studies can be more easily conducted on the Afar margin.

In addition to geologic studies (Wolfenden et al., 2005; Stab et al., 2016), the Afar crust has been imaged along rift with seismic refraction survey (Makris and Ginzburg, 1987). The crustal thickness variations and internal seismic structure of Afar margin have to date been imaged with low resolution using receiver function studies from seismic networks with sparse station spacing (~40-km) (Dugda et al., 2005; Dugda and Nyblade, 2006; Hammond et al., 2011; Kibret et al., 2019). None of the previous studies offer a sufficiently good image of the crustal structure across the margin to unravel the extensional history and any along-margin variations in the role of tectonics and magmatism during the continental breakup.

A detailed image of the finite deformation will help to constrain the structure and evolution of the margin prior and coeval with the continental rifting and answer some of the remaining questions: Does the stretching and the thinning of the continental lithosphere occur over a narrow or broad region? Is the rifting smooth or stepped? What are interactions between mechanical stretching and thinning of the lithosphere, and magma intrusions (e.g. Keir et al., 2013)?

In order to resolve the high-resolution crustal structure of the western margin of the Afar Depression for the first time we analyze data from 24 temporary broadband stations distributed along two densely sampled profiles going from the

western plateau to central and northern Afar. We use P-to-S receiver functions (Burdick and Langston, 1977; Langston, 1977; Ammon, 1991) to image the crust-mantle transition and intracrustal discontinuities as well as to infer crustal properties from Vp/Vs values. This allows us to understand the spatial relationships between plate stretching, thinning and magma intrusion during continental breakup. The comparison of the crustal structure along the two profiles allows us to estimate the longitudinal variations of the rifting along the margin and the respective role of tectonics and magmatism.

2. Background

2.1 *Geological and Tectonic Settings*

Rifting along the Gulf of Aden initiated ~34 Ma ago (Leroy et al., 2012) followed by the emplacement of voluminous Ethiopia-Yemen Trap Series on the Ethiopian and Yemeni plateaus ~31-29 Ma ago (Baker et al., 1996a; Hofmann et al., 1997; Ukstins et al., 2002). On the Ethiopian plateaus, they erupted and covered a thick series of Mesozoic sedimentary rocks (Bosworth et al., 2005; Beyene and Abdelsalam, 2005) currently outcropping on the western plateau, overlying the Neoproterozoic crystalline basement rocks (e.g. Alemu et al., 2018; Le Gall et al., 2018; Fig. 1). They also likely covered parts of the region that would become the Afar Depression.

The initiation of rifting within the Afar is thought to have begun at ~29-26 Ma postdating the main flood basalt event. Geological studies from the central and southern parts of the western margin of Afar propose three main stages of strain migration from the border faults to the current magmatic segments (Wolfenden et al., 2005; Stab et al., 2016). In stage 1, starting just after the flood basalt deposits of 29 to 26 Ma, narrow half-grabens initiate the rift, coeval with the emplacement of rhyolites in these basins. Stage 2 (16-7 Ma) corresponds to the eastward migration of extensional deformation towards the rift axis, and accompanied by fissural basaltic volcanism. Finally, Stage 3 (<7 Ma) includes a further eastward jump in the locus of extension and increase in localized magma intrusion and

voluminous basalts. Stage 3 is responsible for eruption of a ~1.5-km-thick Stratoid Series lava pile of mostly basalts emplaced at 4.0-1.1 Ma that now covers 70% of Afar (Varet, 1975; Stab et al., 2016; Fig. 1). After 1.1 Ma, the deformation and magmatism became localized within discrete seismically and volcanically active magmatic segments characterized by intense diking and volcanism (e.g. Barberi et al., 1972; Abdallah et al., 1979; Hayward and Ebinger, 1996; Manighetti et al., 1998; Wright et al, 2006; Grandin et al., 2009).

Extensional basins in southern and central Afar are filled with Pliocene–Recent lacustrine and fluviatile sedimentary rocks interbedded with basaltic and felsic lava flows (Tesfaye et al., 2003). In northern Afar, the Danakil basin is known to include at least 1 km of Holocene-Recent evaporites (e.g. Bastow et al., 2018; Le Gall et al., 2018). However, the sedimentary basin likely extends to 3-5 km depth with Pliocene-Pleistocene-Recent age evaporites and basalt flows (Bastow and Keir, 2011; Keir et al., 2013).

The western Afar margin preserves the rift morphology since the onset of the flood basalt till the initiation of the seafloor spreading (Tesfaye, et al., 2003; Wolfenden, et al., 2005; Keir, et al., 2013; Ebinger, et al., 2017; Rooney, et al., 2018). This margin is characterized by stratigraphic and structural changes from the south toward the north (e.g. Keir et al., 2013). For example, south of latitude 13°N, the transition from the western plateau, covered here by a thick sequence of Trap series, to the extended crust in the Afar Depression corresponds to a zone of antithetic faults forming a wide zone of marginal basins (Wolfenden et al., 2004, 2005; Stab et al., 2016) . North of latitude 13°N, where the Trap series does not outcrop on the western plateau, the margin is characterized by normal faults forming a narrow zone of marginal grabens (Justin-Visentin and Zanettin, 1974; Kieffer et al., 2004: Wolfenden et al., 2005; Rooney et al., 2018; Le Gall et al., 2018). The seismic activity is more intense in this area with several events of magnitude greater than 5.0 (Ayele et al., 2007; Illsley-Kemp et al., 2018). These changes along the Afar margin are spatially associated with a northward thinning of the crust within the rift, and surface area of Holocene volcanism (Barberi and Varet, 1977; Berckhemer et al., 1975; Makris and Ginzburg, 1987; Hammond et al., 2011; Bastow and Keir, 2011).

2.2 ***Previous constraints on crustal structure***

Previous geophysical studies have contributed significantly to our knowledge of the crustal structure of our study area. Estimates of the crustal thickness and crustal composition beneath Afar and surrounding plateaus have been made using controlled source seismic profiling (Makris and Ginzburg, 1987), inversion of gravity data (e.g. Tiberi et al. 2005) and magnetotelluric imaging (e.g. Desissa et al., 2013). Passive seismic techniques such as P-to-S and S-to-P receiver functions (e.g. Hammond et al., 2011; Lavayssiere et al., 2018), surface waves tomography (e.g. Gallacher et al., 2016) and ambient noise tomography (e.g. Korostelev et al., 2015; Chambers et al., 2019).

Makris and Ginzburg (1987) used the data from an along strike seismic refraction profiles to propose a four-layer crustal structure within the Afar Depression underlain by an anomalous upper mantle (P_n velocity of 7.4-7.5 kms^{-1}). This model consists of a 3-5 km sedimentary cover (a P-wave velocity, Vp of 3.35-3.95 kms^{-1}), that overlies a basaltic layer (Vp=4.5 kms^{-1}) on an abnormally thin upper crust (Vp of 6.1-6.2 kms^{-1}) and a lower crust (Vp of 6.7-7.0 kms^{-1}). This study shows that the crust thins from 26 km in the south and central Afar to 14 km in the north. Crustal thickness inferred from gravity data (Makris et al., 1991; Tiberi et al. 2005), shows thin crust beneath the Afar rift (14-23 km) and thick (~40 km) continental crust beneath the western plateau that is partly intruded with high-density material.

Previous P-to-S receiver function studies (Dugda et al., 2005; Stuart et al., 2006; Hammond et al., 2011; Reed et al., 2014; Kibret et al., 2019; Wang et al., 2021) and a joint inversion of Rayleigh wave velocities and receiver functions (Dugda et al., 2007) confirm these variations, showing ~26-20 km thick crust beneath the Afar Depression and rapidly thinning to ~16 km beneath the Danakil Depression of northern Afar (e.g. Hammond et al., 2011). The estimated crustal thickness beneath the western and southern plateaus range from 36 to 45 km (Dugda et al., 2005; Stuart et al., 2006; Cornwell et al., 2010; Hammond et al., 2011; Kibret et al., 2019; Wang et al., 2021) . These studies also show a normal to elevated Vp/Vs ratio for the plateaus and reaching very high values (Vp/Vs > 2.0) near the

magmatic segments where the crustal thickness is less than 26 km (e.g. Hammond et al., 2011; Wang et al., 2021). A seismic anisotropy study (Hammond, 2014) shows that the melt beneath the Afar Depression is stored in interconnected stacked sills within the lower crust consistent with high Vp/Vs ratios more than 1.95 obtained by receiver functions, an interpretation supported by slow lower crustal S-wave velocities imaged using ambient noise tomography (e.g. Chambers et al., 2019; Korostelev et al., 2015). In addition, S-to-P receiver functions identify a velocity decrease with depth at 65-75 km beneath the western plateau interpreted as the lithosphere-asthenosphere boundary (LAB; Rychert et al., 2012; Lavayssiere et al., 2018). The LAB is not imaged below Afar and interpreted as evidence for melt percolation into the mantle lithosphere (Rychert et al., 2012; Lavayssiere et al., 2018).

However, the seismic stations used in the previous studies (Dugda et al., 2005; Stuart et al., 2006; Hammond et al., 2011; Lavayssière et al., 2018; Chambers et al., 2019; Wang et al., 2021) were deployed at a spacing of several tens of kilometers and those used by Reed et al. (2014) were located along a profile across the south-eastern part of central Afar. Thus, these studies are limited in providing high-resolution images of the crustal structure from the continental stable plateaus to the active rift axes.

3. Data and Methodology

3.1 *Data*

From May 2017 to September 2018, a network including 9 SEIS-UK broadband seismic stations (7 Guralp CMG-3ESPD-60s and 2 CMG-40T-30s with Guralp CMG-DCM datalogger) and 20 French Sismob-RESIF broadband seismic stations (Guralp CMG-40T-30s with Nanometrics Taurus digitizer) were deployed along two SW-NE oriented profiles, more or less perpendicular to the large fault scarps forming the western Afar margin and the main axis of the Afar rift (Fig. 1). This network has been configured to image the crustal structure across the transition from the western plateau to the currently active rifts of the northern and central parts of Afar (Fig. 1). For northern Afar we used 8 stations (N001 to N008) deployed along

an 86 km-long profile spaced by an average distance of 11 km (Keir et al., 2017; Fig. 1). For central Afar we used 15 stations (S001, S003 to S009, S011 to S014, S017, S018 and S020) deployed along ~225 km-long profile spaced by either ~20 km at the ends or ~10 km in the middle of the profile (Doubre et al., 2021; Fig. 1). For improved continuity of the southern profile, we added data from FINE station installed from March 2007 to November 2009 (Ebinger, 2007). All stations recorded continuous data with a sampling rate of 100 Hz except FINE, which recorded continuous data at 50 Hz.

For the receiver function analysis, the IRIS earthquake catalog was searched for events with magnitude ≥ 5.5 Mb, occurring within an epicentral distance range of 30°-95° from the center of the network. To increase the azimuthal coverage, regional events between 20° and 30° were also included (e.g. Park and Lavin, 2001; Salmon et al. 2011; Fig. 2d), with a specific treatment detailed in section 3.2.1. In total, waveforms from 186 earthquakes including 11 regional events have been selected.

SAC software (Goldstein, et al., 2003; Goldstein and Snoke, 2005), TauP toolkit (Crotwell et al. 1999) and the 1D IASP91 velocity model (Kennett and Engdahl, 1991), were used to pick the P-wave arrival time and to prepare the raw seismic data for receiver function analysis. The data were manually inspected and rated based on the signal-to-noise ratio (S/N; the ratio between the amplitude of the signal at P-arrival time to the maximum amplitude of the 5 s pre-arrival noise window), only low-noise traces (S/N > 4) with clear P wave arrival recorded at each station were kept for further analysis. This process resulted in the selection of ~126 earthquakes (including 11 regional events) for receiver function construction and processing (Fig. 2d). After removing the mean and the first-order trends from the selected waveforms, the data were filtered using a zero-phase Butterworth bandpass filter with corner frequencies of 0.02–0.8 Hz and windowed 5 s before and 35 s after the theoretical P arrival time. We then rotated the horizontal seismograms into a great-circle path from the ZNE coordinate system to the ZRT coordinate system.

3.2 *Methods*

3.2.1 *P-to-S receiver functions*

The receiver function technique is widely used to image seismic discontinuities beneath a seismic station by deconvolving the vertical component from the radial and/or transverse components. This aims to remove the instrument response, the propagation path and the source mechanism effects from a broadband teleseismic record (Langston, 1977; 1979). We used the iterative time domain deconvolution technique of Ligorria and Ammon (1999) to compute the receiver functions with 200 iterations. We used a Gaussian width factor of 2.5 in the deconvolution of the vertical trace to predict the radial one (Ligorria and Ammon, 1999), except for noisy stations for which we used a Gaussian width factor of 2.0 to excluded high frequency noise above ~1 Hz. The percentage of recovery was evaluated from the rms misfit between the original radial waveform and the radial receiver function convolved with the vertical component. If the final deconvolution reproduces less than 80 % of the signal, then the event is discarded from further analysis. From this together with a visual inspection for coherence and stability, the number of receiver functions included in the final analysis varies between 15 and 72 per station (Table 1), depending on the background noise and the state of health of the station.

Extra care is required if using regional events in receiver function analysis. They are susceptible to complex P-wave arrivals due to upper mantle triplications (e.g., Chu et al., 2012). To check for any artifacts due to triplicated phases, we only kept the events that will not change the H and/or Vp/Vs beyond the error limits determined from the teleseismic events alone. For example, station S005 has the maximum number of 10 regional events, whereas for most of the other stations they are less than six. Figures S1b,c shows the RFs and H-k plots from station S005 with and without the regional events included, respectively. The estimated crustal thickness and Vp/Vs are approximately the same. Similarly, figure S1d, shows binned and stacked receiver functions in epicentral distance of 10° for three stations that have six or more regional events. It is clear that the results from

regional events (20°-30°) are comparable to the results from teleseismic events (30°-95°) for each station.

3.2.2 *H–κ Stacking*

To determine the average crustal properties, we analyzed receiver functions for each station using the H-κ domain stacking technique of Zhu and Kanamori (2000). This method enables the determination of Moho depth (H) and the velocity ratio of crustal P and S phases (Vp/Vs, or κ) by considering the crust as a homogeneous, horizontal, isotropic layer over a half-space. The inherited trade-off in the receiver function analysis between the crustal thickness (H) and the average crustal velocity properties can be partially resolved using the H-κ stacking algorithm (Ammon et al., 1990), assuming a good assumption can be made about the average P-wave velocity from nearby refraction profiles (e.g. Makris and Ginzburg, 1987). With this information, we sum amplitudes of the receiver functions at predicted arrival times for the Moho P-to-S conversion phase Pms and its multiple converted phases, PpPs and PpSs+PsPs using different weights and a range of H and Vp/Vs values.

The stacking amplitude in the H-k domain is given by:

$$s(H, \kappa) = \sum_{m=1}^{n} w_1 r_m(t_{p_s}) + w_2 r_m\left(t_{p_p p_s}\right) + w_3 r_m\left(t_{p_p S_s + p_s P_s}\right) \quad (1)$$

where n is the number of the radial receiver functions at each station, W_j is a weighting factor that represents the contribution of the direct conversion from the Moho and its multiples according to signal-to-noise ratio ($W_1 + W_2 + W_3 = 1$) and $r_m(t)$ is the amplitude of the point on the receiver function at predicted arrival time t (after the first P arrival) of the associated seismic phase corresponding to the crustal thickness H and Vp/Vs. The stacking amplitude reaches its maximum as the three phases stack coherently, and represents the best estimate for both H and Vp/Vs (κ) beneath the station. Globally, we follow the same weighting factor scheme W_1=0.7, W_2=0.2 and W_3=0.1 of Zhu and Kanamori (2000) that balance the contribution of each phase proportional to low signal-to-noise ratio of multiples. We modified the weighting factors in a few cases, by increasing those for multiples when the Moho conversion phase amplitude is low (W_1=0.5, W_2=0.3 and W_3=0.2:

N008; Figs. 2 and 3) or when high-amplitude intra-crustal interface conversion phases obscured the Moho Pms conversion (W_1=0.4, W_2=0.3 and W_3=0.3: N002; Fig. 2), or by decreasing them when the multiples are less clearly identifiable (W_1=0.8, W_2=0.1 and W_3=0.1: S018: Fig. 2).

The Vp/Vs ratio derived from the H-κ stacking method are related to the elastic parameter Poisson's ratio (σ) through the simple relationship $\sigma = 0.5(1-\{1/[(V_P/V_S)^2 - 1]\})$ (Zandt and Ammon 1995; Ligorria 2000), and is typically used to provide important constraints regarding the bulk crustal composition (e.g. Christensen, 1996; Chevrot and van der Hilst, 2000). Poisson's ratio variations mainly depend on mineralogical composition of the crust (felsic, mafic) and/or the presence of fluids rather than on pressure or temperature conditions (Christensen, 1996; Watanabe, 1993).

3.2.3 ***Results stability and Uncertainty Estimates***

Three important factors control the stability of the H-κ inversion results using the receiver function method: 1) the average crustal P-wave velocity used to do the inversion; 2) the back-azimuth coherency of the Moho converted phase Pms and multiples PpPs and PpSs+PsPs and 3) the level of noise in the receiver function waveform data.

Average crustal P-wave velocity (Vp) used in previous receiver function studies in Ethiopia shows a large range of values (4.6 kms^{-1} - 6.5 kms^{-1}). For example, Dugda et al. (2005) used constant average crustal velocity Vp = 6.5 kms^{-1}. Stuart et al. (2006) used three different Vp values constrained from the EAGLE controlled-source profile of 6.1 kms^{-1}, 6.15 kms^{-1} and 6.25 kms^{-1} for the southern, central Ethiopian rifts, and adjacent plateaus, respectively. Hammond et al. (2011) used values of 6.15 kms^{-1} and 6.25 kms^{-1} for the stations in Afar and on the Ethiopian plateaus again based on nearby refraction profiles (Makris and Ginzburg, 1987). Finally, the average crustal velocity used by Reed et al. (2014) ranges from 4.8 kms^{-1} to 5.9 kms^{-1} based on the comparison of the stacking results using different initial Vp values ranging from 4.5 kms^{-1} to 7.0 kms^{-1} and theoretical Vp versus κ curve. In this study, we used Vp = 6.3 kms^{-1} for the stations located on the western plateau and 6.0 kms^{-1} for the stations located within the Afar rift based on the

controlled-source experiments (Berckhemer et al., 1975; Makris et al., 1975; Makris and Ginzburg, 1987; Mackenzie et al., 2005; Maguire et al., 2006), and the average crustal velocity constraints from the previous receiver function studies (Dugda et al., 2005; Stuart et al., 2006; Hammond et al., 2011; Reed et al., 2014).

To estimate the standard deviation for both crustal thickness H and Vp/Vs, we employ the bootstrap resampling technique (Efron and Tibshirani 1986). The bootstrap analysis was done by repeating the stacking procedure 200 times with random data subsets that are resampled versions of the original data set for each station. The 2σ for each station is shown by error bars in the depth sections and supporting information. The same technique was applied to estimate the errors introduced to the results from the assumed average crustal P-wave velocity used to determine the bulk crustal parameters (H and Vp/Vs; Tiberi et al., 2007). We recalculate H and Vp/Vs values using different average crustal Vp in the range 5.8-6.8 kms^{-1} to test the errors introduced by assuming average crustal Vp (Fig. S5). As suggested by several authors (e.g. Mohsen et al., 2005; Nair et al., 2006; Ogden et al., 2019), for crustal thickness of less than 50 km, a Vp variation of 0.1 kms^{-1} will affect the Moho depth by a value less than 1 km.

3.2.4 ***Receiver Function Depth Migration***

The common-conversion point (CCP) technique is a robust method to transfer the receiver functions from the time-domain to the space-domain (e.g. Kind et al., 2002) and image lateral variations of the subsurface discontinuities along a profile. In this study, we perform a common conversion point (CCP) stacking using the Zhu (2000) technique, based on the back projection of the amplitude vector of the receiver functions along the ray paths using a given 1-D velocity model. The 3-D space beneath the profile is binned and the amplitudes of all the radial receiver functions with rays passing through each bin are averaged to get the amplitude for that bin. To create our depth migrated cross-sections along both the northern and southern profiles, we use a 1-D Vp model based on the nearby refraction profiles (Berckhemer et al., 1975; Makris and Ginzburg, 1987; Mackenzie et al., 2005; Maguire et al., 2006) and the IASP91 velocity model (Kennett and Engdahl, 1991).

The Vs model at each station location is deduced from the Vp/Vs results of the current study, constrained by the previous RF studies (Stuart et al., 2006; Hammond et al., 2011; Reed et al., 2014) and Vs models of Chambers et al. (2019). Therefore, the velocity model varies along both profiles and is constrained to maintain the average crustal velocity Vp comparable to that used for H and Vp/Vs calculations. To optimize for the resolution, the CCP depth images are obtained with a bin width of 10 km (equivalent to the estimated width of the first Fresnel zone for an interface at 30 km depth, assuming a signal frequency of 1.2 Hz and S-wave velocity of 3.4 kms^{-1}; e.g. Salmon et al., 2011). The separation between the centers of the bins is set to 2 km to preserve the spatial resolution and the vertical bin width is set to 0.5 km less than the expected vertical resolution equivalent to the half of the minimum wavelength.

4. Results

Most of the stations show a strong and easily identifiable Pms Moho conversion phase on individual and stacked receiver functions (Figs. 2, 3, S1 and S2). The corresponding multiple PpPs, is also identifiable in most cases, but not as consistently visible as Pms, while the latter arrival multiples PpSs+PsPs are often ambiguous and only clearly observed at a few stations. The Moho conversion phase and/or its multiples may be disturbed by reverberations from near surface, low velocity sediment layers and intracrustal and/or upper mantle interfaces at some stations (Figs. 3 and S1). In this study, we present the results ordered and grouped depending on them being on the northern or southern profiles (Fig. 1) and in light of different geological and tectonic features (e.g. Keir et al., 2013).

4.1 Receiver functions observations

Northern profile

For the stations located on the western plateau (N001 to N005), the Pms phase is observed 6 s after the direct P-wave arrival time. Before the Pms phase, i.e. within 1.0-4.0 s after the direct P-wave arrival time, we observe a strong and coherent

negative intra-crustal phase and two positive intra-crustal phases on the majority of the individual (Figs. 3 and S1) and stacked radial receiver functions (Figs. 2 and S2e). The arrival time and amplitude of the first positive phase depends on the back-azimuth (Figs. 3 and S1), and could be a P-to-S conversion at the bottom of a low velocity shallow layer or could suggests anisotropy or dipping layers. The second strong positive phase is interpreted as a conversion from a mid-crustal interface at ~20 km depth. A clear positive and coherent conversion phase (Phs) arrives behind the Moho P-to-S conversion phase (Pms) at ~9.5 s delay time (Fig. S1e), that Levin and Park (2000) associated with the Hales discontinuity and was reported by previous RFs studies beneath Nubian and Arabian continental shields (Sandvol et al., 1998; Park and Levin, 2001; Ayele et al., 2004).

The amplitudes of the transverse components are much smaller than the corresponding radial amplitudes (Fig. 2). The transverse receiver functions show an intracrustal negative and positive energy that is varying over the back-azimuth, which may suggest the presence of anisotropy (Levin and Park, 1997a).

As shown in Fig. 3b, at station N006 the results show a variation in the amplitude and arrival time of the Pms-converted phase on the radial RFs as well as the polarity reversal of the direct P and Pms-converted phases on the transverse RF as a function of the back-azimuth. This suggests the presence of a dipping Moho. The azimuthal RF variations of the reverberated latter phases show a complex pattern which may indicate the presence of 3-D features such as dipping interfaces and seismic anisotropy within the crust. Such complex pattern and the lack of a homogeneous earthquake distribution with back-azimuth, means it is not possible to do a detailed crustal anisotropy analysis.

The data from the stations located within the marginal graben at the eastern end of the northern profile (N007 and N008) show a positive intra-crustal phase in the radial receiver functions at ~ 1.3-1.5 s after the direct P-wave arrival time (Figs. 2, 3 and S1). The most prominent positive phase visible in the majority of both individual and stacked radial receiver functions (Figs. 2, 3 and S1) arrives within a delay time of 3.0-5.0 s after the direct P-wave arrival and is interpreted as the P-to-S conversion phase (Pms) at the Moho discontinuity. At the easternmost station

(N008), we note a clear and strong negative phase arrives following the Pms phase at ~4.0 s delay time after the P-wave arrival (Fig. 2).

Southern profile

The two westernmost stations (S001 and S003) on the western plateau are characterized by a clear Pms Moho conversion phase arriving with a 6.0 s delay time after the first P–wave arrival and multiples within 18-22 s delay time. A clear pre-Moho conversion phase arrives with a 2.9 s delay time after the first P-wave arrival likely originating from an intra-crustal discontinuity between the upper and lower crusts at ~20 km depth. This phase is particularly coherent and stronger in the S003 individual receiver functions and on the stacked receiver functions of the two stations (Figs 2 and 3). The transverse RFs of the stations S001 and S003 show a significant energy associated with a group of positive and negative pulses preceding the Pms Moho conversion phase. At the expected arrival time of the Pms conversion phase the transverse RFs display small positive amplitudes for the events approaching the station from easterly back-azimuths, (Fig. S2a).

The four stations (S004, S005, S006 and S007) positioned within the basin of the foothill area between the western plateau and the marginal graben are characterized by a clear Moho conversion phase (Figs. 1, 2 and S2b). At station S004, the Pms conversion phase arrives with a delay of 5.0 s after the arrival of the direct P phase with PpPs and PsPs multiples arrives at 16.5 s and 21.0 s, respectively. At stations (S005, S006 and S007) the Moho conversion phase Pms and its multiples (PpPs and PsPs) arrive at ~4.0-4.5 s, ~14.8-15.2 s and ~18.5-19.2 s delay time after the first arrival (Figs. 3, S1a and S2b). The transverse RFs show significant energy from intracrustal interfaces and at the expected arrival time of the Pms conversion phase, with the latter characterized by a polarity change for the events approaching the stations from eastern (positive) and western (negative) directions (Fig. S2b).

Stations sampling the marginal graben and Awra plain (S008, S009, S011, S012 and S013) show, a clear Pms conversion phase arrive within a time window of 3.8 to 4.0 s and its multiples PpPs and PsPs arrive at 12.0-12.5 s and 15-16.0 s after

the P-wave arrival time, respectively (Figs. 2, S1a and S2c). The transverse RFs show a significant negative and positive energy between the direct P wave arrival and the Moho converted phase characterized by reversed polarity in comparison with the radial RFs (Fig. S2c).

At the five stations (S014, FINE, S017, S018 and S020), which are located near and within the Afar rift axis, the radial receiver functions have two positive phases within 4 s after the P-wave arrival time (Figs. 2, 3 and S1). The first low amplitude phase arrival has a delay time of 1–1.5 s with respect to the direct P-wave, and is more likely a conversion at the bottom of low velocity shallow layer. We interpret the second strong and coherent phase arrival at a delay time of 3.5-3.8 s after the direct P-wave with corresponding multiples at 10-10.5 s and 13.5-14.5 s, as the conversion from the Moho (e.g. Figs. 2 and S1a and S2d). The transverse RFs characterized by a clear negative and positive energy arrive between the onset of the P-wave and the Pms Moho conversion phase. In addition, we observe a significant positive energy at the expected arrival time of the Pms Moho conversion phase for events approaching from east-southeast directions (Fig. S2d).

4.2 Crustal thickness and Vp/Vs ratio

The H–κ stacking results show a well-defined peak on the H-k plots (Figs 4 and S2). The crustal thickness H and Vp/Vs estimated from receiver function analysis are shown on the topographic maps of Afar in Fig. 5a and Fig. 5b, respectively. The estimated crustal thickness (H) and Vp/Vs ratio using the H-κ stacking technique and associated errors from bootstrap method are shown in Table 1.

Northern Profile

Our crustal thickness estimates for the western plateau range from 37.6±2.3 to 38.8±1.9 km with an average crustal thickness of ~38.0 km. For station N006 located at the eastern edge of the western plateau results show two peaks on the H-κ plot that correspond to discontinuities at ~28.0 km and 37.0 km, in addition to another peak corresponding to an intra-crustal interface at ~20.0 km depth (Fig.

S3). By comparing the Pms piercing points of N006 (H ~28.0 and 37.0 km) with the piercing points of N005 (H ~38 km) and N007 (H ~24 km) as shown by figure S4, it is clear that a crustal thickness of ~37.0 km could be attributed to the plateau side to the west of this station and ~28.0 km for the foothill area to the east. We obtain 24.2 ± 1.5 km (N007) located at the foothill area and 19.4 ± 1.3 km (N008) at the eastern edge of the marginal graben (Figs. 5a and S5).

The Vp/Vs ratio is relatively normal (1.73±0.01-1.79±0.05) for the stations on the western plateau (N001-N005) and for the station (N007) at the western edge of the marginal graben. At the eastern end of the northern profile at the riftward edge of the marginal graben the N008 station shows high Vp/Vs ratio of 1.93 ± 0.02.

Southern Profile

The crustal thickness along the southern profile decreases from the W to E in three steps, such that four different zones of uniform crustal thickness and Vp/Vs ratio could be identified along the profile (Figs. 6 and S7). These zones broadly correlate with the pre-rift crust of the western plateau, the foothill area between the western plateau and the marginal graben, the stretched crust of the marginal graben and Awra plain, and finally the thinned crust within and in the vicinity of the Afar Manda-Harraro rift segment (MHRS) (Figs. 1, S7).

We estimate an average crustal thickness of 42.0 ± 1.0 km for (S001 and S003; first zone) on the western plateau (Figs. 2, 5a and S7). Except for the S004 station located on/or near the steep border faults with a crustal thickness estimated to 37.2 ± 4.0 km, the crustal thickness for (S005-S007; second zone) within the foothill area is 34.0-34.6 km, with an average crustal thickness of 34.2 ± 1.0 km (Figs. 5a, S7 and Table 1).

In the third zone of extended crust beneath the marginal graben and the Awra plain, five stations (S008, S009, S011, S012 and S013) with a spacing of 5-12 km were used to constrain the crustal thickness (Figs. S1, S7). The associated crustal thickness ranges from 27.6 to 28.2 km (Table 1), with an average value of 28.0 km. The H-κ estimates for the crustal thickness of (S014,FINE, S017, S018 and S020;

fourth zone) within and in the vicinity of the rift axis of central Afar range from 23.2 km to 19.6 km (Fig. S7, Table 1), with an average value of 21.0 ± 1.0 km.

Our Vp/Vs ratios for the southern profile could be grouped into two main groups of the western marginal area and central rift area. Eleven stations located within the western marginal area, eight of them associated with intermediate crustal composition show elevated Vp/Vs ratios in the range from 1.79 to 1.87 and three stations located within the second zone of the foothill area, show low to normal Vp/Vs ratios in the range 1.72±0.03 to 1.76±0.02. On the eastern end of the southern profile, data from S014, FINE, S017, S018 and S020 stations located to the west and within the MHRS show high Vp/Vs ratio of 1.95±0.05, 1.99±0.02, 1.96±0.02, 1.92± 0.01 and 2.02±0.01, respectively (Figs. 5b and S7).

4.3 ***Depth Migrated Profiles***

Figure 6 shows the migrated receiver functions along the northern and southern profiles. The Moho depth obtained from the H-k stacking method of Zhu and Kanamori (2000) and corrected for the station elevation is plotted with error bars from the bootstrap technique of Efron and Tibshirani (1986).

Northern profile

For the northern profile, the Moho interface appears as a strong positive phase (indicated by the red color, Fig. 6a) and can be easily traced. It is almost horizontal beneath the western plateau (N001-N006) at an average depth of ~36 km, and then rises in two gradual changes to a depth of ~18 km below the eastern end of the profile. The first crustal thinning (~14 km vertically over ~10 km horizontally) occurs at the edge of the plateau between N006 station located on the western plateau and N007 station located at the foot of the escarpment within the marginal graben zone. The second crustal thinning occurs within the marginal graben zone between the stations N007 and N008, (~5 km vertically over 15 km horizontally). The crust continues to thin eastward to <15 km towards Dallol within the Danakil Depression (Makris and Ginzburg, 1987; Tiberi et al., 2005; Bastow and Keir, 2011; Hammond et al., 2011; Illsley-Kemp et al., 2017).

Southern profile

The SW-NE-migrated image along the southern profile (Fig. 6b) shows a clear conversion from the Moho at a depth range from ~39-40 km at the western end to ~19-20 km beneath the eastern limit of the profile. The first locus of the crustal thinning occurs at the edge of the escarpment from 42 km beneath the western plateau to ~34 km beneath the foothills zone (8 km vertically over 20 km laterally). The second locus occurs between S007 and S008 stations located at the foothills zone and the marginal graben zone, respectively, reaching an average crustal thickness of 28 km (6 km vertically over 10 km horizontal distance). The last locus of the crustal thinning is at the western edge of the Sullu-Adu range located at the eastern half of Awra basin reaching an average crustal thickness of ~21 km beneath the MHRS at the latitude ~12°N.

5 *Discussion*

5.1 *Comparison with previous estimates of the crustal structure*

Northern Profile:

Our crustal thickness estimate of ~38 km for the western plateau of the northern profile is in a good agreement with the previous receiver functions (~39.0 km; Hammond et al., 2011; Ogden et al., 2019; Fig. 7), and from gravity inversion (~35.0-38.0 km; Makris et al., 1991 ; Tiberi et al., 2001). Similarly, our Vp/Vs values ~1.70-1.79 are consistent with the results of ~1.71-1.77 for the stations ADYE and SMRE (Hammond et al., 2011; Ogden et al., 2019; Fig. 8). The crustal thickness obtained from S-to-P receiver functions (Lavayssiere et al., 2018), and ambient noise tomography (Chambers et al., 2019) is thinner than the crustal thickness estimated by the current study, and likely the crustal thickness is underestimated in their studies (e.g. see Lavayssiere et al., 2018 for a discussion on this). At the eastern end of the northern profile, the crustal thickness and Vp/Vs ratio of 19.4±1.3 km and 1.93±0.02 for N008 compare favorably with the values of 20.0±2.0 km and 1.98±0.1 for the nearby station HALE (Hammond et al., 2011; Figs. 7, 8).

Southern Profile:

Our estimated average crustal thickness of 42.0 km for the elevated western plateau is in good agreement with the previous P-to-S receiver functions results (38-44 km; Dugda et al., 2005; Stuart et al., 2006; Cornwell et al., 2010; Hammond et al., 2011; Kibret, et al., 2019; Wang et al., 2021), with the crustal thickness results from joint inversion of surface waves and Pms receiver functions (~40 km; Dugda et al., 2007), with the estimates from seismic refraction profiles (40-45 km; Makris and Ginzburg, 1987; Mackenzie et al., 2005; Maguire et al., 2006) and crustal thickness from gravity inversion (~40 km; Tiberi et al., 2005). For the marginal area (marginal graben and Awra plain), our estimates of the crustal thickness of ~28.0±1.4 km are consistent with the previous P-to-S receiver function results (~25.0-29.0±1.3 km; Hammond et al., 2011).

Our Vp/Vs results of ~1.79-1.87±0.03 for most of the stations on the western plateau and within the marginal area of central Afar (southern profile) are similar to the results from the previous receiver function studies (~1.81-1.85±0.05; Hammond et al., 2011; Dugda et al., 2005; Figs. 8, S7). Regarding the stations at the foot of the escarpment (half graben basin; southern profile), our Vp/Vs values of ~1.72-1.76±0.03 are consistent with the results obtained by Dugda et al. (2005) and Hammond et al. (2011) for the nearby station DIYA.

In the easternmost zone within and in the vicinity of the rift axis of central Afar, the crustal thickness and Vp/Vs results (~21.4±1.7 and 1.99±0.02) are similar to the results obtained by Hammond et al. (2011) using the same data at the station FINE. For the other stations our average crustal thickness value of 21.0±1.0 km is in a good agreement with result obtained by Hammond et al. (2011) and Reed et al. (2014) (Fig. 7). Similarly, our high Vp/Vs values above 1.9 are comparable to the results for the nearby stations obtained by Hammond et al. (2011) and less than the values estimated by Reed et al. (2014) for the region to southeast of our stations (Fig. 8). The higher values of Reed et al. (2014) may be the result of the assumed average crustal velocity used in the receiver function analysis of ~5.1 kms^{-1}.

5.2 ***Crustal thicknesses and architecture***

5.2.1 ***Western Plateau***

For the stations located on the western plateau, observations of the high amplitude coherent Moho converted arrivals and consistent estimated crustal thickness beneath the western plateau stations of each profile indicate that the Moho interface is mostly flat beneath the western plateau, while the intra-crustal conversions are laterally variable in amplitude and depth at some stations. A recent study of Ogden et al. (2019) show that the reliability of the high frequencies RFs results are very low at the center of the flood-basalt province where the gradational Moho thickness is >13.0 km and such reliability increases toward the outside of the flood-basalt. However, they concluded that H–κ stacking maintains reliability at low frequencies when the gradational Moho thickness is less than 13.0 km. Their study did not include results from the stations located nearby to our stations. At the southern part of the western plateau, the wide-angle reflection/refraction results at the latitude of the Main Ethiopian Rift (MER) show a ~47.0 km thick crust. This study constrained the thickness of the high-velocity layer at the bottom of the lower crust to be ~15.0 km with clear reflections from the top and bottom of this layer and an apparent velocity of (7.4 kms^{-1}). Cornwell et al. (2010), show that the high-velocity layer thins northeastward from 18.0 to 6.0 km with clear Pms conversions from the top and the bottom of the layer.

Our receiver function (calculated with both a maximum frequency of ~0.6 and ~1.2 Hz; e.g. Cassidy, 1992; Julia et al., 2005) from the station located at the eastern edge of the western plateau along the southern profile does not show double peak Pms phase (Figs. 3a, d and S2a). Instead, it shows a large amplitude intracrustal phase and Pms converted phase with a lag time of (6s), the latter consistent with the Pms phase from the bottom of the high-velocity layer of Cornwell et al. (2010), as well as a strong crustal reverberation (Fig. 3d). Our results are consistent with a recent receiver function study, which yielded the highest stacking amplitude values for the western plateau nearby to our stations (Wang et al., 2021). This indicates that the Moho beneath the stations on the western plateau is flat with a large change in seismic velocity contrast between the

crust and the mantle and does not allow us to constrain the thickness of the intruded high-velocity layer. This could be due to a thin intruded layer (< 4.0 km) below the vertical resolution owing to the wavelength of the incoming plane waves and/or to a low velocity contrast between this layer and the overlying part of the lower crust. However, if the crust-mantle transition is not a sharp boundary, our estimated crustal thickness depends on the long wavelength of the teleseismic waves we use, and more likely to select the center of the crust-mantle transition gradient (e.g. Ogden et al., 2019). In that case, we estimate the crustal thickness (include the magmatic additions) to be ~45.0-46.0 km in comparison with the average crustal thickness of ~38.0 km for the plateau beneath the northern profile (off-flood-basalt stations). In fact, the Jurassic sediments (pre-flood basalts surface) lies at an average altitude of ~2200 m (Gani et al., 2007), and the higher topography (~3700 m) of the western plateau at the latitude of the southern profile is due to the emplacement of ~1500-1800 m-thick flood-basalts deposits at the top of the Jurassic sediments. Hence, if the crust-mantle transition is a sharp boundary, then this has the implication that the western plateau still under dynamic support process as proposed by Sembroni et al. (2016). On the other hand, if the crust-mantle is a gradational boundary of ~8.0 km thickness, the implications are that the western plateau is locally compensated with magmatic additions at the base of the lower crust as Tiberi et al. (2005) concluded from interpretation of gravity and seismic data.

Most of the western plateau stations of the northern and southern profiles show a clear intra-crustal conversion phase with a lag time of ~2.9-3.0 s from a mid-crustal discontinuity at ~20.0-21.0 km depth, likely showing the upper crust-lower crust boundary beneath the western plateau, similar to the discontinuity mentioned by Hammond et al. (2011). Toward the southern part of the western plateau at the latitude of the Main Ethiopian Rift (MER), a clear intracrustal interface is modeled by the active seismic profile. This interface separates the upper and lower crust with Vp of 6.1-6.4 kms^{-1} and 6.6-7.1 kms^{-1}, respectively (Makris and Ginzburg, 1987; Mackenzie et al., 2005; Maguire et al., 2006). A similar interface has been reported and interpreted as the Conrad discontinuity in

previous receiver function studies of the eastern Red Sea conjugate margin of Yemen and southeastern Gulf of Aden margin (Ahmed et al., 2013, 2014). It was estimated at the same depth of ~21.0 km beneath the Yemeni high plateau covered by the Cenozoic continental flood basalts (Ahmed et al., 2013). Previous seismic refraction profiles across the Arabian shield confirm the existence of this interface between the upper crust with an average Vp of 6.3 kms^{-1} and the lower crust with an average Vp of 7.0 kms^{-1} (Mooney et al., 1985; Egloff et al. 1991). This discontinuity suggests a mafic composition for the lower crust, likely altered by magmatic intrusions or partial melt as a result of Miocene-Oligocene flood basalt and the ongoing magmatic activity (Hammond et al., 2011; Ahmed et al., 2013). Interestingly, this interface is almost imaged at the same depth of 20-21 km beneath the Arabian shield, beneath Jordan (Mooney et al., 1985; Stern and Johnson, 2010; and references therein), beneath Yemen plateau (Ahmed et al., 2013) and beneath the western plateau in this study. Although the exact physical meaning of this discontinuity is not clear, it is most likely separates the slower brittle upper crust from the faster ductile lower crust (Stern and Johnson, 2010).

Our Vp/Vs values for the undeformed northern part of the western plateau with 1000-2000 m sedimentary cover are below 1.80 with an average value of ~1.74. This is lower than the global average of 1.77 and best explained by Precambrian crust of felsic to intermediate compositions (Zandt and Ammon, 1995; Christensen, 1996), which is lacking significant magmatic modification before or during the breakup (Christensen and Mooney, 1995; Thompson et al., 2010; Ogden et al., 2019).

The western plateau at the latitude of the southern profile is characterized by elevated Vp/Vs values which may indicate that the lower crust composition has been modified due to mafic intrusions associated with the Cenozoic flood basalts (Hofmann et al., 1997; Pik et al., 1999; Cornwell et al., 2010; Hammond et al., 2011), partial melt in the lower crust (Hammond et al. 2011; Ahmed et al. 2013), or be fluids circulation within the upper crust (Keir et al., 2009; Korostelev et al., 2015; Chambers et al., 2019).

5.2.2 Crustal thinning and composition across western Afar margin

Northern Afar

For the first time we create a high resolution profile of the crustal structure across the northern Afar margin into the Danakil Depression that offers an opportunity to interpret the rifting evolution leading to the establishment of the currently highly active segment of a divergent plate boundary. Taking into account the previous constraints on the crustal thickness near Erta'Ale rift zone and the Dallol Depression deduced by Makris and Ginzburg (1987) and Hammond et al. (2011), the variations of the Moho depth estimated in this study can be extended from the margin to the active rift axis.

The onset of the crustal extension occurs at the ~1400 m high escarpment between N006 and N007 stations, (i.e. between 39.8°E-39.9°E; Figs. 1, S6) with ~14.0 km vertical thinning over ~10.0 km horizontal distance. The crustal thinning continues eastward in two more gradient changes before the crust reaches a thickness of ~14.0 km at the rift axis (Berckhemer et al., 1975; Makris and Ginzburg, 1987). We note that, the lateral change of the crustal thickness across the western margin of northern Afar shows comparable crustal thickness variations to that beneath Yemen which is the eastern Red Sea conjugate margin of Ethiopia, with ~35.0 km beneath the Yemen plateau, ~22.0 km for the Yemen coastal plain and a lowest value of ~14.0 km on the Yemen Red Sea coast (Ahmed et al., 2013; Fig. 7).

Our close station spacing allows us to constrain the locus of the crustal extension more precisely than previous studies. Assuming a pre-rift crustal thickness of 38.0 km beneath the western plateau, a crustal thickness of ~19.0 km beneath the marginal graben and reaching the final thickness of ~14.0 km at the rift axis, we estimate a stretching factor β of ~2.0 for the marginal graben and β of ~2.7 for the northern Afar area between the western plateau and the rift axis. This factor obtained for northern Afar is slightly higher than the maximum value obtained for the Yemen Red Sea conjugate margin (β ~ 2.5, Ahmed et al., 2013).

There is a clear eastward change of the Vp/Vs ratio from low-to-intermediate values, below the western plateau and the area at the foot of the escarpment (<

1.80) to high values for the area near the eastern border faults of the marginal graben (> 1.90), and reaching very high values (>2.0) at the current rift axis (e.g. Hammond et al., 2011). The high Vp/Vs ratio we found for the station N008 indicates an important change in the bulk composition of the crust due to mafic intrusions along the eastern boundary antithetic faults of the marginal graben (Illsley-Kemp et al., 2018; Zwaan et al., 2020b) or could be due to the existence of crustal fluids. The reported eastward increase in the Vp/Vs ratios toward the rift axis (Hammond et al., 2011) suggests more mafic/ultramafic material and/or may indicate a partial melting within the crust increasing with proximity of the rift axis. This is consistent with observations of recent magma intrusion related ground deformation at the axis of the Danakil Depression (e.g. Nobile et al., 2012; Pagli, et al., 2012).

The structure of the northern Afar margin has been primarily controlled by a stretching phase in the early stages of continental rifting c.a ~26-20 Ma (Ukstins et al., 2002; Wolfenden et al., 2005), most likely related to the extension induced by the divergence between Arabian and Nubian plates. It should be noted that during this tectonic event the thickness of both the upper crust and lower crust decreases by a factor of two. This is evident from the depth of the mid-crustal discontinuity dropping from ~20.0 km beneath the western plateau to ~9.0-10.0 km beneath the eastern edge of the marginal graben (station N008; Figs. 6a, S2e). In the late stages of continental rifting after 11 Ma the extension between the marginal grabens and the rift axis is accommodated by thinning of the upper crust by a factor of 2, while the lower crustal thickness remains constant. This is also evident from the mid-crustal discontinuity at ~5.0 km beneath the Danakil Depression (Makris and Ginzburg, 1987). This significant thinning of the upper crust over short length scales is consistent with geological constraints suggesting that rifting along the marginal area of northern Afar associated with upper crustal extension and dominant tectonic deformation (Bastow & Keir, 2011; Keir et al., 2013; Bastow et al., 2018). In contrary, an increase in rift magmatism associated with dike intrusions confined to the rift axis has initiated relatively recently (Quaternary) in the evolution of the rifting of northern Afar (e.g. Bastow and Keir, 2011; Nobile et al., 2012; Pagli et al., 2012).

Central Afar

Unlike the northern profile, in central Afar the number of stations along our southern profile allows us to continuously image the Moho depth and to constrain the crustal composition variations from the western plateau to the rift axis. The crustal thickness decreases eastward by ~8.0 km over ~20.0 km horizontal distance between the western plateau and the second zone located at the foot of the ~1700 m high escarpment. Then it decreases in two more steps by ~6.0 km and ~7.0 km over ~10.0 km horizontal distance from the second to the third and to the fourth zones, respectively (Fig. S7). The estimated β factors between these zones are 1.24, 1.21 and 1.30 respectively. We estimate an overall β of 2.1 for central Afar assuming an initial crustal thickness of ~42.0 km beneath the western plateau and a final crustal thickness of ~20.0 km (S020) at the eastern end of the profile. Our estimated stretching factor β for central Afar is comparable with the estimate from the previous receiver function studies (Hammond et al., 2011) but remains smaller than the β value of 3.0 and 2.7 predicted from plate reconstructions (Wolfenden et al., 2005) and from cross section balancing (Stab et al., 2016), respectively. The discrepancy between our estimated β and the predicted β is best explained by magmatic addition to the crust during extension (e.g. Thybo and Nielsen, 2009; Stab et al., 2016). This implies 4.0 or 5.0 km of magmatic addition depending on the predicted β value used.

Most of the stations located within the western marginal area of central Afar (southern profile) show elevated Vp/Vs ratios which suggest intermediate to mafic composition except three stations that show low to normal Vp/Vs ratios. The latter with low to normal values are located within the foothill area and reflect that the Precambrian felsic crust has been poorly contaminated or intruded by mafic rocks. These low Vp/Vs values could also result from the emplacement of felsic volcanic strata coincidence with the onset of faulting along the central Afar margin (26-22 Ma; Wolfenden et al., 2005; Ayalew et al., 2019), and/or that the crust has been intruded by granitic plutons (fast S-wave mantle material) such as along the Yemen conjugate margin (Hughes and Beydoun, 1992; Davison et al., 1994; Geoffroy et al., 1998; Ahmed et al., 2013). The slightly elevated values for the other

stations that are distributed in the marginal graben and the Awra plain may indicate that the lower crust composition has been modified due to mafic intrusions associated with the Cenozoic flood basalts (Hofmann et al., 1997; Pik et al., 1999; Cornwell et al., 2010; Hammond et al., 2011), partial melt in the lower crust (Hammond et al., 2011; Ahmed et al., 2013; Wang et al., 2021), fluids circulation within the upper crust (Keir et al., 2009; Korostelev et al., 2015; Chambers et al., 2019), or thick sedimentary deposits within the basin (Stab et al., 2016).

Finally, at the vicinity and within the MHRS, the significant increase in the Vp/Vs ratio is coincident with the thin crust (20.0 km) toward the central axis of the rift. Such high values of Vp/Vs ratio above 1.90 are very rare (except for few minerals like serpentine) and likely indicate a small amount of partial melt and/or fluids in the crust (Watanabe, 1993; Christensen, 1996; Zandt and Ammon, 1995). Hammond et al. (2011) used receiver function forward modeling for three stations located west and northwest of MHRS (to the north of our stations) to show that partial melt in the lower crust may exist beneath regions of thinner crust of central Afar. Reed et al. (2014) used the theoretical velocity-melt relationship developed by Watanabe (1993) for granitic rocks with rhyolitic melt, to estimate 4.2-11.4% melt fraction at the location of their stations located in central Afar to the southeast of our stations.

Additional observations supporting the existence of partial melt within the crust at the vicinity and within the MHRS come from imaged slow shear wave velocities within the crust and the uppermost mantle beneath the magmatic segments (Hammond et al., 2011; Stork et al., 2013; Korostelev et al., 2015; Chambers et al., 2019), magnetotelluric results that also point to a wide conductive zones within the crust beneath MHRS interpreted as a large magma volumes that contains ~13% melt fraction (Desissa et al., 2013; Didana, et al., 2014; Johnson et al., 2016) and recent series of dike intrusions at MHRS (Keir et al., 2013). Finally, Hammond (2014) invert H-κ data at three stations within and in the vicinity of MHRS for melt fraction and anisotropy and show that the melt is likely stored in the form of stacked sills within the lower crust with a maximum thickness of 2.8 km and connected by some melt inclusions in preferential vertical alignment. Hammond

(2014) shows that the anisotropy, and resultant amplitude dominance of the slow shear wave in H-k stacking is a likely cause of the high Vp/Vs ratios for the average crust of the MHRS.

The crustal structure variations across the western margin of central Afar are consistent with the distinct geological and structural domains of this region. From the west, the early stretching stage of the continental rifting (c.a ~26-23 Ma; correspond to first step of the Moho interface between S003 and S004; second zone; Fig. S7) occurs below the main escarpment. This stretching phase is characterized by large offset normal fault, distributed over a wide area (Stab et al., 2016) and accompanied with the formation of the half graben basin at the foot of the escarpment and the emplacement of felsic magmatism (Wolfenden et al., 2005). The following extension event occurs ~30.0 km eastward below the western bounding faults of the marginal graben and corresponding to the second step of the Moho interface from the second to the third zones (between S007 and S008; Fig. S7). This extension event occurs after the emplacement of many Miocene giant dykes within and in the vicinity of the marginal graben (Chorowicz et al., 1999; Stab et al., 2016; Ayalew et al., 2019; Zwaan et al., 2020b). Zwaan et al. (2020a, b) suggest that this event is related to the rotation of the Danakil block and dated from geological studies as between 16-7 Ma (Wolfenden et al., 2005; Zwaan et al., 2020a, b). During this extension event the stretching was distributed over a wide area, most likely accompanied with the formation of antithetic normal faults and NE tilted blocks were created (Stab et al., 2016). A third extension event occurs below the western edge of Sullu-Adu range (between S013 and S014; Figs., 1, S7). This event was accompanied with uplift of the Sullu-Adu area, subsidence of the Awra plain and extensive magmatism (Bosworth et al., 2005; Stab et al., 2016). However, the results deduced from our dense network of stations indicate a differential extension between the brittle and ductile layers of the crust, such that the upper crust thins from ~21.0 beneath the western plateau to ~7.0 km beneath the fourth zone, whereas the lower crust thins from ~21.0 km to ~12.0 km. Hence, these observations requires a décollement or ductile fault surfaces to accommodate the upper crust lower crust differential extension and distribute the upper crust extension over a wide area.

5.3 ***Implications for the evolution of the rifting***

Continental rifting leading to continental breakup and oceanic spreading encompasses a complex interplay of extensional faulting, thinning of the crust and lithosphere and intrusive-extrusive magmatism (Buck, 2004; Geoffroy, 2005; Lavier and Manatschal, 2006; Cannat et al., 2009; Leroy et al., 2010; Nonn et al., 2019). Because of the geological observations that have been preserved in Afar due to the subaerial context of the region and because the rifting is not complete yet, the results on the crustal structure and the Vp/Vs ratios along our two profiles help to discriminate between the possible mechanisms of extension involved during the formation of the margin, over the specific period from the onset of the rifting, i.e. ca. 26 Ma, to the time of the setting up the Stratoïd series, i.e. ca. 4-2 Ma. Separated by only ~150.0 km with a major transfer zone (EATZ; Fig. 1), the two sections along the western Afar margin show strong dissimilarities in their deep structure, particularly regarding the geometry of the Moho depth across the margin. The two sections differ primarily by the amount of the stretching and the width of the extended area from the western plateau to the rift axis. In northern Afar, the stretching factor β of the brittle crust and ductile lower crust is ~4.0 and ~2.0, respectively, whereas in central Afar β is ~3.0 for the brittle crust and ~1.6 for the ductile lower crust. The sharp decrease in the crustal thickness between the western plateau and the marginal graben during the early stages of extension (β ~ 2.0 and 1.5 for the northern and central Afar, respectively) suggests different rate of the mechanical extension that has been accommodated by large border faults. During the latter stages of extension between the marginal graben and rift axis, the differential thinning between the brittle and ductile crustal layers suggests that the two layers were decoupled and associated with mechanical extension in the brittle crust and ductile flow in the lower crust (e.g. Jolivet et al., 2015). In northern Afar, the extension during these latter stages is accommodated by the thinning of the upper crust only and distributed over a narrow extended area (~40 km). This is consistent with the high Vp/Vs ratio, the thin seismogenic layer (~5 km; Craig et al., 2011; Nobile et al., 2012) and the thin effective elastic thickness (Te ~6 km; Ebinger and Hayward, 1996; Pérez-Gussinyé et al., 2009;

Ebinger et al., 2017). The stretching and thinning across the western margin of central Afar occurs on a wide distance (>100 km), accommodated by thinning of both the upper and lower crust and associated with decrease in crustal thickness by three successive steps from the stable continental western plateau to the active rift axis. Whereas the Vp/Vs ratios do not show any correlation with the crustal thickness and/or age, but well correlate to the mafic intrusions and increased melt within the crust. These observations are consistent with a rifting history at the latitude of central Afar dominated by a discontinuous riftward migration of the extensional strain over time associated with intense magmatism (Wolfenden et al., 2005; Stab et al., 2016).

Geological evidences across the margin of central Afar show that stretching and thinning phases took place between extensive magmatic pulses, during the Oligocene pre-rift period (main continental flood basalt; ~31-29 Ma), late Oligocene-early Miocene (Miocene Basalts and Rhyolites; ~25-22 Ma), late Miocene (Miocene Basalts and Rhyolites; ~9-7 Ma) and the Pliocene (Stratoid series; ~5-2 Ma; Stab et al., 2016). Our results provide compositional and spatial constraints with multiple crustal thinning steps consistent with the hypothesis of episodic thinning and related magmatic cycles from the western plateau down to the active central Afar magmatic segment.

The along-strike variations of the structure of the margin evidenced at depth by our results but also at surface from several geological studies (Wolfenden et al., 2005; Bastow and Keir, 2011; Stab et al., 2016; Le Gall et al., 2018) can be interpreted as the result of a difference of stage of the continental breakup evolution associated with a distinct conditions in which the continental extension occurs, such as the local strain rate and/or the depth and the temperature of the upper mantle which change the rheology of the crust and of the lithospheric mantle. This different rheological behavior is marked by the major transfer zone (EATZ) and on either sides of this transfer zone, we note the important variability of the magma supply.

7. Conclusion

We use the receiver function technique and teleseismic data recorded by a temporary broadband seismic array deployed along two profiles crossing the western margin of Afar to constrain the tectonic processes that are involved in the evolution of the rift. Our results provide constraints on the following characteristics of the crustal thickness and composition:

(1) The crustal thickness beneath the western plateaus is 37-43 km, and decreases eastward to its minimum ranges from 14-23 km beneath the central rift axis. The decrease in the crustal thickness is more pronounced beneath the foothills and marginal grabens, but the crust also thins elsewhere in discrete steps. This is consistent with jumps in strain localization during rifting, rather than progressive strain migration. The crustal thinning of northern Afar points towards a β of 2.7, and in central Afar of 2.2. Both values are lower than a β of 3.0 predicted by plate reconstructions, with the discrepancy best explained by 2-5 km of magmatic addition to the crust. The amount of crustal thinning is higher in northern Afar, pointing towards increased plate stretching in the north.

(2) The Vp/Vs ratios suggest that the crustal composition along the western margin of Afar could be classified with unmodified crust with felsic to normal crustal composition, (western plateau next to northern Afar), altered crust due to magmatic intrusion and/or additions (western plateau and marginal area of central Afar) and highly modified crustal composition associated with the presence of partial melt at the central rift axis.

(3) There is a significant difference between the western margin characteristics of the northern Afar (Danakil Depression) in comparison with the western margin of the central Afar. In northern Afar, the crustal extension occurs over a short distant associated with significant thinning of the upper crust and dominant tectonic deformation. In central Afar, the crustal extension occurs on a wide area and characterized by episodic crustal thinning associated with intense magmatic activity.

(4) The elevated Vp/Vs ratios are generally associated with the crustal thicknesses of less than 21 km, in or near the active magmatic segments showing the role of the magmatic processes in the final stages of continental rifting.

Acknowledgments

Data used in this study were collected by the AFAR17 project in Ethiopia. The instruments for the project were provided by the French National Research Infrastructure SISMOB-RESIF (http://www.resif.fr) and SEIS-UK. RESIF is supported by the Ministry of Higher Education and Research. The facilities of SEIS-UK are supported by the Natural Environment Research Council (NERC) under agreement R8/H10/64. Funding for fieldwork (deployments, data collection and maintenance) is from Sorbonne Université, ISTEP, Institute des Sciences de la Terre de Paris. AA is supported by the University of Sorbonne (iSTeP), the University of Strasbourg (FACE program) and the PAUSE program. DK is supported by NERC grant NE/L013932/1, and MIUR grant PRIN 2017P9AT72. We wish to thank the Addis-Abeba University staff for help in customs clearance and for the technical facilities, the Afar Regional Authorities and local people for their kind cooperation and their help to make the fieldwork successful. We deeply thank, Alex Nercessian, IPGP, the Centre Français d'Etudes Ethiopiennes (CFEE) in Addis-Ababa for the help and support provided by the center during the experiment.

References

Abbate, E., Sagri, M. 1969. Dati e considerazioni sul margine orientale dell'altiplano etiopico nelle province del Tigrai e del Wollo. Boll Soc Geol It 88, 489–497.

Abdallah, A. et al., 1979. Relevance of Afar seismicity and volcanism to the mechanics of accreting plate boundaries, Nature, 282, 17–23.

Ahmed, A., Tiberi, C., Leroy, S., Stuart, G. W., Keir, D., Sholan, J., Khanbari, K., Al-Ganad, I. and Basuyau, C. 2013. Crustal structure of the rifted volcanic margins and uplifted plateau of Western Yemen from receiver function analysis, Geophys. J. Int., 193(3), 1673–1690, doi:10.1093/gji/ggt072.

Ahmed A., Leroy, S., Keir, D., Korostelev, F., Khanbari, K., Rolandone, F., Stuart, G., Obrebski, M., 2014. Crustal structure of the Gulf of Aden southern margin: Evidence from receiver functions on Socotra Island (Yemen), Tectonophys., 637, 251-267, doi: 10.1016/j.tecto.2014.10.014., 337, 251-267.

Alemu, T., Abdelsalam, M. G., Dawit, E. L., Atnafu, B., & Mickus, K. L. (2018). The Paleozoic e Mesozoic Mekele Sedimentary Basin in Ethiopia: An example of an exhumed IntraCONtinental sag (ICONS) basin. J. Afr. Earth Sci., 143, 40 –58. https://doi. org/10.1016/j.jafrearsci.2018.03.010

Ammon, C.J., Randall, G. and Zandt, G., 1990. On the nonuniqueness of receiver function inversions, J. Geophys. Res., 95, 15 303–15 318.

Ammon, C.J., 1991. The isolation of receiver effects from teleseismic P waveforms, Bull. Seism. Soc. Am., 81, 2504–2510.

Ayalew, D., Pik, R., Bellahsen, N., France, L., & Yirgu, G. (2019). Differential fractionation of rhyolites during the course of crustal extension, Western Afar (Ethiopian rift). Geochem. Geophys. Geosyst. 20, 571–593. https://doi.org/10.1029/2018GC007446

Ayele, A., G. Stuart, and J. Kendall (2004), Insights into rifting from shear wave splitting and receiver functions: An example from Ethiopia, Geophys. J. Int., 157(1), 354–362.

Ayele, A., Stuart, G., Bastow, I., and Keir, D., 2007. The August 2002 earthquake sequence in north Afar: Insights into the neotectonics of the Danakil microplate. J. Afr. Earth Sci., 40, 70–79.

Baker, J. A., L. Snee, and M. Menzies, 1996a. A brief Oligocene period of flood volcanism in Yemen: Implications for the duration and rate of continental flood volcanism at the Afro-Arabian triple junction, Earth Planet. Sci. Lett., 138(1), 39–55.

Bellahsen, N., S. Leroy, J. Autin, P. Razin, E. d'Acremont, H. Sloan, R. Pik, A. Ahmed, and K. Khanbari (2013), Tectonophysics, Tectonophysics, 607(C), 32–50, doi:10.1016/j.tecto.2013.07.036.

Barberi, F., and Varet, J., 1977. Volcanism in the Afar Depression: small-scale plate tectonic implications, Bull. Geol. Soc. Amer., 88, 1251-1266.

Barberi, F., Tazieff, H. and Varet, J., 1972. Volcanism in the Afar Depression: Its tectonic and magmatic significance. Tectonophys., 15, 19-29, https://doi.org/10.1016/0040-1951(72)90046-7

Barnie, T. D., Keir, D., Hamling, I., Hofmann, B., Belachew, M., Carn, S., ...Vye-Brown, C. (Ed.), 2016. A multidisciplinary study of the final episode of the Manda Hararo dyke sequence, Ethiopia, and implications for trends in volcanism during rifting cycle. Geo. Soc. London, Spec. Pub., 420, 149-163. doi: 10.1144/SP420.6

Bastow, I., and Keir, D., 2011. The protracted development of the continent ocean transition in Afar. Nat. Geosc., 4(4), 248–250. https://doi.org/10.1038/ NGEO01095

Bastow, I. D., Booth, A. D., Corti, G., Keir, D., Magee, C., Jackson, C. A.-L., etal., 2018. The development of late-stage continental breakup: Seismic reflection and borehole evidence from the Danakil Depression, Ethiopia. Tectonics, 37, 2848–2862. https://doi.org/10.1029/ 2017TC004798

Berckhemer, H., et al., 1975. Deep seismic soundings of the Afar region and on the highland of Ethiopia, in Afar Depression of Ethiopia: Proceedings of an International Symposium on the Afar Region and Related Rift Problems, Held in Bad Bergzabern, FR Germany, April 1–6, 1974, pp. 89–107, Schweizerbart, Stuttgart, Germany.

Beyene, A., and. Abdelsalam M. G, 2005. Tectonics of the Afar Depression: A review and synthesis, J. Afr. Earth Sci., 41, 41–59.

Black, R., Morton, W.H., Varet, J., 1972. New data on Afar Tectonics. Nat. Phys. Sci. 240, 170–173. https://doi.org/10.1038/physci240170a0.

Bosworth, W., Huchon, P., and McClay, K. 2005. The Red Sea and Gulf of Aden Basins, J. Afr. Earth. Sci., 43, 334–378.

Brisbourne, A., 2012. How to store and share geophysical data. Astron. Geophys., volume 53,19-20

Buck, W.R., 2004. Consequences of asthenospheric variability on continental rifting. In: Karner, G., Taylor, B., Driscoll, N.W. and Kohlstedt, D.L. (Eds), Rheology and deformation of the lithosphere at continental margins. Columbia University Press, New York, 1-30

Burdick, L.J. and Langston, C.A., 1977. Modeling crustal structure through the use of converted phases in teleseismic body waveforms, Bull. Seism. Soc. Am., 67, 677–692.

Cannat, M., Manatschal, G., Sauter, D. and Péron-Pinvidic, G., 2009. Assessing the conditions of continental breakup at magma-poor rifted margins: What can we learn from slow spreading mid-ocean ridges? C. R. Geosci. 341, 394–405.

Cassidy, J.F., 1992. Numerical experiments in broad-band receiver function analysis, Bull. seism. Soc. Am., 82, 1453–1474.

Chambers, E. L., Harmon, N., Keir, D., & Rychert, C. A. (2019). Using ambient noise to image the northern East African Rift. Geochem. Geophys. Geosyst., 20, 2091–2109. https://doi. org/10.1029/2018GC008129

Chevrot, S., and R. D. van der Hilst (2000), The Poisson ratio of the Australian crust: Geological and geophysical implications, Earth Planet. Sci. Lett., 183, 121 – 132.

Christensen, N. I., 1996. Poisson's ratio and crustal seismology, J. Geophys. Res., 101, 3139–3156.

Christensen, N.I. and Mooney, W.D., 1995. Seismic velocity structure and composition of the continental crust: a global view. J. Geophys. Res. 100, 9761–9788.

Chu, R., Schmandt, B. and Helmberger, D.V., 2012. Upper mantle P velocity structure beneath the Midwestern United States derived from triplicated waveforms. Geochem. Geophys. Geosyst., 13.

Clark, S. A., F. Niu, A. Levander, and the BOLIVAR Working Group, 2006. Tearing the lithosphere: Diachronous slab detachment along the Venezuelan margin from BOLIVAR seismic data, Eos Trans. AGU, 87, Fall Meet. Suppl., Abstract, T42C-06.

Cornwell, D. G., Magurie, P. K. H., England, R. W. and Stuart, G. W., 2010. Imaging detailed crustal structure and magmatic intrusion across the Ethiopian rift using a dense linear broadband array, Geochem. Geophys. Geosyst., 11, Q0AB03, doi:10.1029/2009GC002637.

Courtillot, V., 1982. Propagating rifts and continental breakup. Tectonics, 1: 239-250.

Crotwell, H. P., T. J. Owens, and J. Ritsema, 1999, The TauP Toolkit: Flexible seismic travel-time and ray-path utilities, Seismo. Res. Lett., 70, 154–160, doi:10.1785/gssrl.70.2.154.

Chorowicz, J., Collet, B., Bonavia, F., Korme, T., 1999. Left-lateral strike-slip tectonics and gravity induced individualisation of wide continental blocks in the western Afar margin. Eclogae Geol. Helv. 92, 149–158. https://doi.org/10.5169/seals-168656.

Craig, T. J., Jackson, J. A., Priestley, K. and McKenzie, D., 2011. Earthquake distribution patterns in Africa: Their relationship to variations in lithospheric and geological structure, and their rheological implications, Geophys. J. Int., 185, 403–434, doi:10.1111/j.1365-246X.2011.04950.x.

d'Acremont. E., Leroy. S., Beslier. M.O., Bellahsen. N., Fournier. M., Robin C., Maia. M., Gente. P., 2005. Structure and evolution of the eastern Gulf of Aden conjugate margins from seismic reflection data. Geophys J Int 160:869–890

d'Acremont, E., Leroy, S., Maia, M., Patriat, P., Beslier, M.O., Bellahsen, N., Fournier, M., Gente, P., 2006. Structure and evolution of the eastern Gulf of Aden: insights from magnetic and gravity data (Encens-Sheba/MD117 cruise). Geophys. J. Int. 165:786–803

Daniels, K. A., Bastow, I. D., Keir, D., Sparks, R. S. J. and Menand, T., 2014. Thermal models of dyke intrusion during development of continent-ocean transition. Earth planet. Sci. Lett., 385, 145-153. doi: 10.1016/j.epsl.2013.09.018

Davison, I. et al., 1994. Geological evolution of the southeastern Red Sea Rift margin, Republic of Yemen, Geol. Soc. Am. Bull., 106, 1474–1493.

Desissa, M., Johnson, N. E., Whaler, K. A., Hautot, S., Fisseha, S., and Dawes, G. J. K., 2013. A mantle magma reservoir beneath an incipient mid-ocean ridge in Afar, Ethiopia. Nat. Geosc., 6, 861-865.

Didana, Y. L., Thiel, S. and Heinson, G., 2014. Magnetotelluric imaging of upper crustal partial melt at Tendaho graben in Afar, Ethiopia, Geophys. Res. Lett., 41, 3089–3095, doi:10.1002/2014GL060000.

Doubre C., A. Déprez, A., Masson, F., Socquet, A., Lewi, E., Grandin, R., Nercessian, A., Ulrich, P., De Chabalier, J., Saad, I., Abayazid, A., Peltzer, G., Delorme, A., Calais, E. and Wright, T., 2017. Current deformation in Central Afar and triple junction kinematics deduced from GPS and InSAR measurements, Geophys. J. Int. 208, 936–953.

Doubre, C., Leroy, S., Keir, D., Pagli, C. and RESIF, 2021. Study of the structure of the lithosphere from the continental plateau of western Ethiopia to the active Afar rift (RESIF-SISMOB)[Data set] RESIF. Reseau Sismologique et Géodésique Francais.

Dugda, M., Nyblade, A., Julià, J., Langston, C., Ammon, C., and Simiyu, S., 2005. Crustal structure in Ethiopia and Kenya from receiver function analysis. J. Geophys. Res., 110, B01303. doi.org/10.1029/2004JB003065

Dugda, M. T., and Nyblade, A. A. (2006). New contraints on crustal structure in eastern Afar from the analysis of receiver functions and surface wave dispersion in Djibouti. In: The Afar volcanic province within the East African Rift System. Geol. Soc., London Spec. Pub., 259, 239-251.

Dugda, M. T., Nyblade, A. A., & Julia, J. (2007). Thin lithosphere beneath the Ethiopian plateau revealed by a joint inversion of Rayleigh wave group velocities and receiver functions. J. Geophys. Res., 112, B08305. https://doi.org/10.1029/2006JB004918

Ebinger, C.J., Hayward, N.J., 1996. Soft plates and hot spots: views from Afar. J. Geophys. Res. Solid Earth 101, 21859–21876. https://doi.org/10.1029/96JB02118.

Ebinger, C. J., and Sleep N. H., 1998. Cenozoic magmatism throughout east Africa resulting from impact of a single plume, Nature, 395, 788-791.

Ebinger, C. E., and Casey, M. (2001). Continental breakup in magmatic provinces: An Ethiopian example. Geology, 29(6), 527–530.

Ebinger, C. (2007). AFAR. International Federation of Digital Seismograph Networks. https://doi.org/10.7914/SN/ZE_2007

Ebinger, C. J., Keir, D., Bastow, I. D., Whaler, K., Hammond, J. O. S., Ayele, A., … Hautot, S., 2017. Crustal structure of active deformation zones in Africa: Implications for global crustal processes. Tectonics, 36,n3298–3332. https:// doi.org/10.1002/2017TC004526

Efron, B. and Tibshirani, R., 1986. The Bootstrap Method for standard errors, confidence intervals, and other measures of statistical accuracy, Stat. Sci., 1, 1–35.

Egloff, F., Rihm, R., Makris, J., Izzeldin, Y., Bobsien, M., Meier, K., Junge, P., Noman, T. and Warsi, W. 1991. Contrasting structural styles of the eastern and western marginsof the southern Red Sea: The 1988 SONNE experiment, Tectonophys., 198, 329–353.

Gallacher, R., D. Keir, N. Harmon, G. Stuart, S. Leroy, J. Hammond, J-M. Kendall, A. Ayele, B. Goitom, G. Ogubazghi, and A. Ahmed (2016), The initiation of segmented buoyancy-driven melting during continental breakup, Nat. Comms, 7, doi: 10.1038/ncomms13110.

Gani, N. D., Gani, M. R. & Abdelsalam, M. G., 2007. Blue Nile incision on the Ethiopian Plateau: Pulsed plateau growth, Pliocene uplift, and hominin evolution. GSAToday17,4

Geoffroy, L., Huchon, P. and Khanbari, K., 1998. Did Yemeni tertiary granites intrude neck zones of a stretched continental upper crust? Terra Nova, 10, 196–200.

Geoffroy, L., 2005. Volcanic passive margins, C. R. Geoscience, 337, 1395–1408.

Goldstein, P., Dodge, D., Firpo, M., and Minner, Lee, 2003. SAC2000: Signal processing and analysis tools for seismologists and engineers, Invited contribution to The IASPEI International Handbook of Earthquake and Engineering Seismology, Edited by WHK Lee, H. Kanamori, P.C. Jennings, and C. Kisslinger, Academic Press, London.

Goldstein, P., and Snoke, A., 2005. SAC availability for the IRIS community (online), IRIS DMS Newsl., 7(1). (Available at http://www.iris.edu/news/newsletter)

Grandin, R., Socquet, A., Binet, R., Klinger, Y., Jacques, E., de Chabalier, J.-B. and Pinzuti, P., 2009. September 2005 Manda Hararo-Dabbahu rifting event, Afar (Ethiopia): constraints provided by geodetic data, J. geophys. Res., 114, doi:10.1029/2008JB005843

Grandin, R., Socquet, A., Doin, M. P., Jacques, E., de Chabalier, J. B. and King, G. C. P., 2010. Transient rift opening in response to multiple dike injections in the manda hararo rift (Afar, Ethiopia) imaged by time-dependent elastic inversion of interferometric synthetic aperture radar data, J. Geophys. Res., 115, B09403, doi:10.1029/2009JB006883.

Grandin, R., A. Socquet, A., Jacques, E., Mazzoni, N., de Chabalier, J.-B. and King, G. C. P., 2010. Sequence of rifting in Afar, Manda-Hararo rift, Ethiopia, 2005–2009: Time-space evolution and interactions between dikes from interferometric synthetic aperture radar and static stress change modeling, J. Geophys. Res., 115, B10413, doi:10.1029/2009JB000815.

Hagos L, Shomali H, Roberts R. 2006. Re-evaluation of focal depths and source mechanisms of selected earthquakes in the Afar Depression. Geophys. J. Int. 167:297–308

Hammond, J. O. S., Kendall, J.-M., Stuart, G., Keir, D., Ebinger, C., Ayele, A., and Belachew, M., 2011. The nature of the crust beneath the Afar triple junction: Evidence from receiver functions. Geochem. Geophys. Geosyst., 12, Q12004. https://doi.org/10.1029/2011GC003738

Hammond, J. O. S. et al., 2013. Mantle upwelling and initiation of rift segmentation beneath the Afar Depression, Geology, 41, 635–638, doi:10.1130/G33925.1.

Hammond, J. O. S., 2014. Constraining melt geometries beneath the Afar Depression, Ethiopia from teleseismic receiver functions: The anisotropic H-κ stacking technique. Geochem. Geophys. Geosyst., 15, 1316.1332. http://doi.org/10.1002/2013GC005186

Hammond, W. C. and Humphreys, E., 2000. Upper mantle seismic wave velocity: effects of realistic partial melt geometries. J. Geophys. Res. 105, 10975-10986.

Hayward NJ, Ebinger CJ. 1996. Variations in the along-axis segmentation of the Afar rift system. Tectonics 15:244–57.

Hofmann, C., Courtillot, V., Feraud, G., Rochette, P., Yirgu, G., Ketefo, E. and Pik, R., 1997. Timing of the Ethiopian flood basalt event and implications for plume birth and global change, Nature, 389, 838–841.

Hughes, G.W. and Beydoun, Z.R., 1992. The Red Sea–Gulf of Aden: biostratigraphy, lithostratigraphy and palaeoenvironments, J.Petrol.Geol.,15, 135–156.

Illsley-Kemp, F., Savage, M. K., Keir, D., Hirschberg, H. P., Bull, J. M., Gernon, T. M., et al., 2017. Extension and stress during continental breakup: Seismic anisotropy of the crust in northern afar. Earth and Planetary Science Letters, 477, 41–51. https://doi.org/10.1016/j.epsl.2017.08.014

Illsley-Kemp, F., Keir, D., Bull, J. M., Gernon, T. M., Ebinger, C., Ayele, A., et al., 2018. Seismicity during continental breakup in the Red Sea rift of Northern Afar. J. of Geophys. Res.: Solid Earth, 123, 2345–2362. https://doi.org/10.1002/2017JB014902

Jolivet, L., Menant, A., Sternai, P., Rabillard, A., Arbaret, L., Augier, R., Laurent, V., Beaudoin, A., Grasemann, B., Huet, B., Labrousse, L., Le, L., 2015. The geological signature of a slab tear below the Aegean. Tectonophysics 659, 166– 182. doi:10.1016/j.tecto.2015.08.004

Johnson, N.E., Whaler, K.A., Hautot, S., Fisseha, S., Desissa, M. and Dawes, G.J.K. (2016), Magma imaged magnetotellurically beneath an active and an inactive magmatic segment in Afar, Ethiopia. Geol. Soc., London, Spec Pub., 14, 150000. https://doi.org/ 10.1144/SP420.11

Julia, J., Ammon, C.J., and Nyblade, A. A., 2005. Evidence for mafic lower crust in Tanzania, East Africa, from joint inversion of receiver functions and Rayleigh wave dispersion velocities. Geophys. J. Int., 162, 555–569.

Justin-Visentin, E. and Zanettin, B., 1974. Dike swarms, volcanism and tectonics of the Western Afar margin along the Kombolcha-Eloa traverse (Ethiopia). Bull. Volc., 38: 187-205

Keir, D., I. Bastow, K. Whaler, E. Daly, D. G. Cornwell, D. G. and Hautot, S., 2009. Lower-crustal earthquakes near the Ethiopian rift induced by magma

injection, Geochem. Geophys. Geosyst., 10, Q0AB02, doi:10.1029/2009GC002382.

Keir, D., Belachew, M., Ebinger, C., Kendall, J.-M., Hammond, J.O.S., Stuart G.W., Ayele, A., Rowland, J., 2011. Mapping the evolving strain field during continental breakup from crustal anisotropy in the Afar Depression. Nat. Commun. 2, 285.

Keir, D., Bastow, I. D., Pagli, C., and Chambers, E. L., 2013. The development of extension and magmatism in the Red Sea rift of Afar. Tectonophysics, 607, 98–114. https://doi.org/10.1016/j.tecto

Keir, D. (2017). Afar Margin Northern Profile. International Federation of Digital seismograph Network. Https://doi.org/10.7914/SN/YQ_2017

Kennett, B.L.N. and Engdahl, E.R., 1991. Traveltimes for global earthquake location and phase identification, Geophys. J. Int., 122, 429–465.

Kibret, B.A., Ayele, A., Keir, D., 2019. Crustal thickness estimates beneath four seismic stations in Ethiopia inferred from p-wave receiver function studies. J. Afr. Earth Sci. 150, 264-271. https://dx.doi.org/10.1016/j.jafrearsci.2018.11.005.

Kieffer, B., Arndt, N., Lapierre, H., Bastien, F., Bosch, D., Pecher, A., et al. (2004). Flood and shield basalts from Ethiopia: Magmas from the African superswell. Journal of Petrology, 45, 793–834. https://doi.org/10.1093/petrology /egg112

Kind, R., Yuan, X., Saul, J., Nelson, D. and S. Sobolev, S., 2002. Seismic images of crust and upper mantle beneath Tibet: Evidence for Eurasian plate subduction, Science, 298, 1219–1221.

Korostelev, F. et al., 2015. Magmatism on rift flanks: Insights from ambient noise phase velocity in Afar region, Geophys. Res. Lett., 42 ,2179–2188.

Kürsten, O. C. M., 1975. Tectonic inventory of the Danakil Depression, in Afar Depression of Ethiopia, pp. 170–174, eds Pilger, A. and Rösler, A., Schweizerbart'sche Verlagsbuchhandlung, Stuttgart

Lahitte, P., Gillot, P.Y., Kidane, T., Courtillot, V. and Bekele, A., 2003a. New age constraints on the timing of volcanism in central Afar, in the presence of

propagating rifts, J. Geophys. Res., 108(B2), 2123, doi:10.1029/2001 JB001689.

Langston, C.A., 1977. Corvallis, Oregon, crustal and upper mantle structure from teleseismic P and S waves, Bull. seism. Soc. Am., 67, 713–724.

Langston, C.A., 1979. Structure under Mount Rainier, Washington, inferred from teleseismic body waves, J. geophys. Res., 84, 4749–4762.

Laughton, A.S. and Tramontini, C., l969. Recent studies of the crustal structure of the Gulf of Aden, Tectonophys., 8, 359–375.

Lavayssiere, A., Rychert, C. A., Harmon, N., Keir, D., Hammond, J. O. S., Kendall, J. M., et al. (2018). Imaging lithospheric discontinuities beneath the northern East African Rift using S-to-P receiver functions. Geochem. Geophys., Geosyst., 19, 4048–4062. https://doi. org/10.1029/2018GC007463

Lavier, L.L. and Manatschal, G., 2006. A mechanism to thin the continental lithosphere at magma-poor margins. Nature 440:324–328

Le Gall, B., Leleu., S., Pik., R., Jourdan, F., Chazot, G., Ayalew, D., Yirgu G., Cloquet, C. and Chauvet, F., 2018. The Red Beds series in the Erta Ale segment, North Afar. Evidence for a 6 Ma-old post-rift basin prior to continental rupturing. Tectonophys. 747-748, 373–389.Leroy, S. et al., 2012. From rifting to oceanic spreading in the Gulf of Aden: a synthesis, Arab J. Geosci., 5(5), 859–901.

Leroy, S., Ebinger, C., d'Acremont, E., Stuart, G., Al-Lazki, A., Tiberi, C., Autin, J., Watremez, L., Beslier, M.O., Bellahsen, N., Lucazeau, F., Perrot, J., Mouthereau, F., Courrèges, E., Huchon, P., Rouzo, S., Bahalaf, S., Sholan, J., Unternehr, P., Hello, Y., Anglade, A., Desprez, O., Beguery, L., Aouji, O., Daniel, R., Al-Toubi, K., Sage, F., Khanbari, K., 2006. The Onshore–Offshore ENCENS Project: Imaging the Stretching/ Thinning of the Continental Lithosphere and Inception of Oceanic Spreading in the Eastern Gulf of Aden, AGU Fall Meeting, AGU, San Francisco.

Leroy, S. et al. (2010), Contrasted styles of rifting in the eastern Gulf of Aden: A combined wide-angle, multichannel seismic, and heat flow survey, Geochem. Geophys. Geosyst., 11(7):1–14. doi:10.1029/ 2009GC002963

Leroy S, Razin F, Autin J, Bache F, d'Acremont E, Watremez L, Robinet J, Baurion C, Denèle Y, Bellahsen N, Lucazeau F, Rolandone F, Rouzo S, Serra KielJ, Robin C, Guillocheau F, Tiberi C,Basuyau C, Beslier M-O, Ebinger C, Stuart G, Ahmed A, Khanbari K, AlGanad I, de Clarens P, Unternehr P, Al Toubi A, Al Lazki A, 2012. From rifting to oceanic spreading in the Gulf of Aden: a synthesis. Arab J Geosci. http://dx.doi.org/10.1007/s12517-011-0475-4

Levin, V., and J. Park, 1997a. Crustal anisotropy beneath the Ural mtns foredeep from teleseismic receiver functions, Geophys. Res. Lett. 24, 1283–1286.

Levin, V., and Park, J., 2000. Shear zones in the Proterozoic lithosphere of the Arabian Shield and the nature of the Hales discontinuity, Tectonophysics 323, 131–148.

Ligorria, J. and Ammon, G., 1999. Iterative deconvolution and receiver functions estimation, Bull. seism. Soc. Am., 89, 1395–1400.

Ligorria, J.P., 2000. An investigation of the crust-mantle transition beneath North America and the bulk composition of the North American crust, PhD thesis, Saint Louis University, p. 261.

Lister, G.S., Etherdge, M.A., and Symonds, P.A., 1986. Detachment faulting and the evolution of passive continental margins: Geology, v. 14, p. 246-250.

Mackenzie, G. D., Thybo, H. and Maguire, P. K. H., 2005. Crustal velocity structure across the Main Ethiopian Rift: Results from two-dimensional wide-angle seismic modelling, Geophys. J. Int., 162, 994 – 1006.

Maguire, P. K. H., et al., 2006. Crustal structure of the northern Main Ethiopian Rift from the EAGLE controlled-source survey: A snapshot of incipient lithospheric break-up, in The Afar Volcanic Province within the East African Rift System, edited by G. Yirgu, C. J. Ebinger, and P. K. H. Maguire, Geol. Soc. Spec. Publ., 259, 269–292.

Makris, J., H. Menzel, H., Zimmermann, J. and Gouin, P., 1975. Gravity field and crustal structure of northern Ethiopia, in Afar Depression of Ethiopia: Proceedings of an International Symposium on the Afar Region and

Related Rift Problems, Held in Bad Bergzabern, FR Germany, April 1–6, 1974, pp. 135–144, Schweizerbart, Stuttgart, Germany.

Makris, J., and Ginzburg A., 1987. The Afar Depression: Transition between continental rifting and sea-floor spreading, Tectonophys., 141, 199−214

Makris, J., Henke, C.H., Egloff, F. & Akamaluk, T., 1991. The gravity field of the Red Sea and East Africa, Tectonophysics, 198, 369–382. Makris, J., and Ginzburg, A., 1987. The Afar Depression: Transition between continental rifting and sea-floor spread- ing, Tectonophys. 141, 199–214.

Manighetti, I., Tapponnier, P., Gillot, P.-Y., Jacques, E., Courtillot, V., Armijo, R. and King, G., 1998. Propagation of rifting along the Arabia-Somalia plate boundary: Into Afar, J. Geophys. Res., 103, 4947–4974.

McKenzie, D. P., Davies, D. and Molnar, P., 1972. Plate tectonics of the Red Sea and East Africa, Nature, 224, 125–133.

Medynski, S., et al., 2013. Controls on magmatic cycles and development of rift topography of the Manda Hararo segment (Afar, Ethiopia): Insights from cosmogenic 3He investigation of landscape evolution, Earth Planet. Sci. Lett., 367, 133–145, doi:10.1016/j.epsl.2013.02.006.

Medynski, S., et al., 2015. Stability of rift axis magma reservoirs: Spatial and temporal evolution of magma supply in the dabbahu rift segment (Afar, Ethiopia) over the past 30 kyr, Earth Planet. Sci. Lett., 409, 278–289.

Medynski, S., Pik, R., Burnard, P., Dumont, S., Grandin, R., Williams, A., et al. (2016). Magmatic cycles pace tectonic and morphological expression of rifting (Afar Depression, Ethiopia). Earth and Planetary Science Letters, 446, 77 –88. https://doi.org/10.1016/j. epsl.2016.04.01

Mohr, P. (1962). The Ethiopian rift system. Bull. Geophys. Obser., Addis Ababa 5, 33–62.

Mohsen, A., Hofstetter, R., Bock, G., Kind, R., Weber, M., Wylegalla, K., R¨umpker, G. & DESERT Group, 2005. A receiver function study across the Dead Sea Transform, Geophys. J. Int., 160, 948–960.

Mooney, W.D., Gettings, M.E., Blank, H.R. and Healey, J.H., 1985. Saudi Arabian seismic refraction profile: a traveltime interpretation of crustal and upper mantle structure, Tectonophys., 111, 173–246.

McClusky, S., Reilinger, R., Ogubazghi, G., Amleson, A., Healeb, B., Vernant, P., et al., 2010. Kinematics of the southern Red Sea–Afar Triple Junction and implications for plate dynamics. Geophys. Res. Lett., 37, L05301. https://doi.org/10.1029/2009GL041127

Nair, S.K., Gao, S.S., Liu, K.H., Silver, P.G., 2006. Southern African crustal evolution and composition: constraints from receiver function studies. J. Geophys. Res. 111 (B2), 1–17. http://dx.doi.org/10.1029/2005JB003802.

Nobile, A., Pagli, C. Keir, D., Wright, T. J., Ayele, A., Ruch, J. and Acocella, V., 2012. Dike-fault interaction during the 2004 Dallol intrusion at the northern edge of the Erta Ale Ridge (Afar, Ethiopia), Geophys. Res. Lett., 39, L19305, doi:10.1029/2012GL053152.

Nonn, C., Leroy, S., Lescanne, M., Castilla, R., 2019. Central Gulf of Aden conjugate margins (Yemen-Somalia)_ Tectono-sedimentary and magmatism evolution in hybrid-type margins. Marine and Petroleum Geology 105, 100–123. doi:10.1016/j.marpetgeo.2018.11.053.

Ogden, C.S., Bastow, I.D., Gilligan, A. and Rondenay, S., 2019. A reappraisal of the H–κ stacking technique: implications for global crustal structure, Geophys. J. Int., 219, 1491–1513, doi: 10.1093/gji/ggz364.

Pagli, C., Wright, T. J., Ebinger, C. J., Yun, S. H., Cann, J. R., Barnie, T. and Ayele, A., 2012. Shallow axial magma chamber at the slow-spreading Erta Ale Ridge, Nat. Geosci., 5(4), 284–288.

Park, J. & Levin, V., 2001. Receiver functions from regional P waves, Geophys. J. Int., 147, 1–11.

Pérez-Gussinyé, M., Metois, M., Fernandez, M., Verges, J. and Lowry, A.R., 2009. Effective elastic thickness of Africa and its relationship to other prozie for lithospheric structure and surface tectonics. Earth Planet. Sci. Lett., 287(1-2), 152-167. https://doi.org/10.1016/j.epsl.2009.08.004

Pik, R., Deniel C., Coulon C., Yirgu G., Hofmann C., and Ayalew D. (1998). The northwestern Ethiopian Plateau flood basalts: Classification and spatial distribution of magma types. J. Volc. Geotherm. Res., 81, 91-111.

Pik, R., Deniel, C., Coulon, C., Yirgu, G., & Marty, B., 1999. Isotopic and trace element signatures of Ethiopian flood basalts; evidence for plume lithosphere interactions. Geochimica et Cosmochimica Acta, 63(15), 2263–2279. https://doi.org/10.1016/S0016-7037 (99)00141-6

Pik, R. (2011). East-Africa on the rise. Nat. Geosciences, 4, 660-661.

Reed, C. A., Almadani, S., Gao, S. S., Elsheikh, A. A., Cherie, S., Abdelsalam, M. G., Thurmond, A. K. and Liu, K. H., 2014. Receiver function constraints on crustal seismic velocities and partial melting beneath the Red Sea Rift and adjacent regions, Afar Depression, J. Geophys. Res., 119, 2138–2152, doi:10.1002/2013JB010719.

Rooney, T. O., Krans, S. R., Mège, D., Arnaud, N., Korme, T., Kappelman, J., & Yirgu, G. (2018). Constraining the magmatic plumbing system in a zonedcontinental flood basalt province. Geochem., Geophys., Geosyst., 19, 3917–3944. https://doi.org/10.1029/ 2018GC007724

Ruegg, J.C., 1975. Main results about the crustal and upper mantle structure of the Djibouti region (T.F.A.I), in Afar Depression of Ethiopia, pp. 120–134, eds Pilger, A. and Rösler, A., Schweizerbart'sche Verlagsbuchhandlung, Stuttgart.

Salmon, M.L., Stern T.A. & Savage M.K., 2011. A major step in the continental Moho and its geodynamic consequences: the Taranaki–Ruapehu line, New Zealand, Geophys. J. Int., 186, 32–44, doi: 10.1111/j.1365-246X.2011.05035.x

Sandvol, E., D. Seber, A. Calvert, and M. Barazangi (1998). Grid search modeling of receiver functions: implications for crustal structure in the Middle East and North Africa, J. Geophys. Res., 103, 26,899– 26,917.

Sembroni, A., Faccenna, C., Becker, T.W., Molin, P. and Abebe, B., 2016. Longterm, deep-mantle support of the Ethiopia-Yemen Plateau, Tectonics, 35, 469–488, doi:10.1002/2015TC004000.

Smittarello, D., Grandin, R., De Chabalier, J.-B., Doubre, C., D´eprez, A., Masson, F., Socquet, A. and Saad, A., 2016. Transient deformation in the Asal-Ghoubbet Rift (Djibouti) since the 1978 diking event: Is deformation controlled by magma supply rates?, J. Geophys. Res., 121, doi:10.1002/2016JB013069.

Stab, M., Bellahsen, N., Pik, R., Quidelleur, X., Ayalew, D., and Leroy, S., 2016. Modes of rifting in magma-rich settings: Tectono-magmatic evolution of Central Afar., Tectonics, 35, 2–38. https://doi.org/10.1002/2015TC003893

Stern, R.J. and Johnson, P., 2010. Continental lithosphere of the Arabian Plate: a geologic, petrologic, and geophysical synthesis. Earth-Science Reviews 101, 29–67.

Stork, A., G. W. Stuart, C. M. Henderson, D. Keir, and J. O. S. Hammond (2013), Uppermost mantle (Pn) velocity model for the Afar region, Ethiopia: An insight into rifting processes, Geophys. J. Int., 193, 321–328.

Stuart, G.W., Bastow, I.D. and Ebinger, C.J., 2006. Crustal structure of the northern Main Ethiopian Rift from receiver function studies, in The Afar Volcanic Province Within the East African Rift System, Vol. 259, pp. 253-267, eds Yirgu, G., Ebinger, C.J. and Maguire, P.K.H., Geol. Soc., London, Spec Pub..

Tiberi, C., Ebinger, C., Ballu, V., Stuart, G. and Oluma, B., 2005. In- verse models of gravity data from the Red Sea-Aden-East African rifts triple junction zone, Geophys. J. Int., 163, 775–787, doi:10.1111/j.1365-246X.2005.02736.x.

Tiberi, C., Leroy, S., d'Acremont, E., Bellahsen, N., Ebinger, C., Al-Lazki, A. and Pointu, A., 2007. Crustal geometry of the northeastern Gulf of Aden passive margin: localization of the deformation inferred from receiver function analysis, Geophys. J. Int., 168, 1247–1260.

Tesfaye, S., Harding, D., and Kusky, T., 2003. Early continental breakup boundary and migration of the Afar triple junction, Ethiopia. Geol. Soc. of Amer. Bull., 115(9), 1053–1067. https://doi.org/10.1130 /B25149.1

Tesfaye, S., Ghebreab, W., 2013. Simple shear detachment fault system and marginal grabens in the southernmost Red Sea rift. Tectonophys. 608, 1268–1279. https:// doi.org/10.1016/j.tecto.2013.06.014.

Thompson, D.A., Bastow, I.D., Helffrich, G., Kendall, J.M., Wookey, J., Snyder, D.B. & Eaton, D.W., 2010. Precambrian Crustal Evolution: Seismic constraints from the Canadian Shield, Earth, Planet. Sci. Lett., 297, 655-666. doi: 10.1016/j.epsl.2010.07.021

Thybo, H., and C. A. Nielsen (2009), Magma-compensated crustal thinning in continental rift zones, Nature, 457, 873–876, doi:10.1038/ nature07688.

Ukstins, I. A., Renne, P. R., Wolfenden, E., Baker, J., Ayalew, D. and Menzies, M., 2002. Matching conjugate volcanic rifted margns: 40 Ar/ 39 Ar chrono-stratigraphy of pre- and syn-rift bimodal flood volcanism in Ethiopia and Yemen, Earth Planet. Sci. Lett., 198, 289–306.

Varet, J., 1975. Carte géologique de l'Afar central et méridional, CNR- CNRS, 1/500 000 Géotechni.

Wang, T., Gao, S.S., Yang, Q. and Kelly H., 2021. Crustal structure beneath the Ethiopian Plateau and adjacent areas from receiver functions: Implications for partial melting and magmatic underplating. Tectonophysics (2021), https://doi.org/10.1016/ j.tecto.2021.228857

Watanabe, T., 1993. Effects of water and melt on seismic velocities and their application to characterization of seismic reflectors, Geophys. Res. Lett., 20, 2933–2936.

Wolfenden, E., Ebinger, C., Yirgu, G., Deino, A. and Ayalew, D., 2004. Evolution of the northern Main Ethiopian rift: Birth of a triple junction, Earth Planet. Sci. Lett., 224, 213–228, doi:10.1016/j.epsl.2004.04.022.

Wolfenden, E., Ebinger, C., Yirgu, G., Renne, P. R. and Kelly, S. P., 2005. Evolution of a volcanic rifted margin: Southern Red Sea, Ethiopia, Geol. Soc. Am. Bull., 117, 846–864.

Wright, T. J., Ebinger, C., Biggs, J., Ayele, A., Yirgu, G., Keir, D. and Stork, A., 2006. Magma-maintained rift segmentation at continental rupture in the 2005 Afar dyking episode, Nature, 442, 291–294, doi:10.1038/ nature04978.

Zandt, G. and Ammon, C.J., 1995. Continental crust composition constrained by measurement of crustal Poisson's ratio, Nature, 374, 152–154.

Zhu, L., 2000. Crustal structure across the San Andreas Fault, Southern California from teleseismic converted waves, Earth planet. Sci. Lett., 179, 183–190.

Zhu, L. and Kanamori, H., 2000. Moho depth variation in Southern California from teleseimic receiver function, J. Geophys. Res., 105, 2969–2980.

Zwaan, F., Corti, G., Keir, D., Sani, F., 2020a. A review of tectonic models for the rifted margin of Afar: implications for continental break-up and passive margin formation. J. Afr. Earth Sci. 164, 103649. https://doi.org/10.1016/j.jafrearsci.2019.103649.

Zwaan, F., Corti, G., Sani, F., Keir, D., Muluneh, A. A., Illsley-Kemp, F., & Papini, M., 2020b. Structural analysis of the Western Afar Margin, East Africa: Evidence for multiphase rotational rifting. Tectonics, 39, e2019TC006043. https://doi.org/10.1029/ 2019TC006043

Zwaan, F., Corti, G., Keir, D., and Sania, F., 2020c. Analogue modelling of marginal flexure in Afar, East Africa: Implications for passive margin formation. Tectonophys., 796, 228595. https://doi.org/10.1016/j.tecto.2020.228595.

Tables and Figures

Table1. Crustal thickness (H), Vp/Vs ratio for the seismic stations and associated uncertainty estimates deduced from the bootstrap analysis.

Figure 1. Topographical map of the study area showing the main tectonic structures and the location of the seismic stations (red triangles) along two profiles from the western plateau to the central rift axis. MHRS: Manda Harraro Rift Segment. Inset at the upper right corner is a structural map of the Afar Depression and surrounding highlands modified from Stab et al. (2016) and Le Gall et al. (2018), with a regional map show the location of the study area.

Figure 2. Stacked radial (dark/grey fill colour) and transverse (red/blue fill colour) receiver functions for the 23 seismic stations along two profiles. a) the southern profile at the latitude of the central Afar, and b) the northern profile - Danakil Depression, c) sketch illustrating the path of the converted phases and d) map showing the distribution of the ~126 teleseismic events selected and used for receiver functions analysis in this study centered at the network location.

Figure 3. a) Individual receiver functions for six stations. The receiver functions are organized by increasing backazimuth (value in red). The light vertical lines indicate arrival times for conversion phases (Pms and multiples) from the Moho for the maximum stacking amplitude; ; b) Ps radial RFs at the N006 seismic station for good quality data within an epicentral range 30°-95°, stacked in backazimuth into bins of 15° and with an overlap of 5°. The numbers of RFs in each stack are indicated above each trace to the left and the backazimuth ranges to the right; c) Ps transverse RFs at the N006 seismic station stacked with the same epicentral distance, backazimuth ranges and number of RFs in each stack as in b; d) Stacked Ps radial RFs with a maximum frequency of 0.6 Hz (red line) and 1.2 Hz (blue line) at the S003 seismic station located at the eastern edge of

the western plateau southern profile (central Afar). The stacked transverse RFs with a maximum frequency of 1.2 Hz is represented by a dashed black line.

Figure 4. Thickness (H) versus Vp/Vs ratio diagrams from the H-k stacking method for the 6 stations presented in Figure 4. The white point indicates the maximum stacking corresponds to the value indicated in Table 1. The scale bar is the amplitude of stacking function.

Figure 5. Maps of crustal thicknesses (H) and Vp/Vs ratios calculated using the H-k method; a) Topographical map with the crustal thickness variations across western Afar margin and b) Topographical map with the Vp/Vs ratios across the western Afar margin. MHRS: Manda Harraro Rift Segment.

Figure 6. Topography (vertically exaggerated) and migrated cross-sections along the two profiles. Red colour indicates velocity increase with depth, and blue colour velocity decrease with depth. Scale bar shows the amplitude of positive (red) and negative (blue) polarities of arrivals. The Moho depth estimated from H-k stacking method and corrected for the station altitude is plotted with the small circles and the vertical bars represent the errors estimated from the bootstrap method. a) Northern profile – Northern Afar and b) Southern profile – central Afar.

Figure 7. Regional map showing crustal thickness (H) based on the results of the current study (white circles) and previous RF studies in Ethiopia (red triangles, Hammond et al. 2011; inverted white triangles, Stuart et al., 2006; magenta pentagon, Dugda et al., 2005), RF in Yemen (white stars, Ahmed et al. 2013). Active seismic profiles (+ sign), in Afar (Berckhemer et al., 1975; Makris and Ginzburg, 1987), in the Red Sea (Egloff et al., 1991), in the Western Gulf of Aden (Laughton and Tramontini, 1969) and in Djibouti (Ruegg, 1975).

Figure 8. Regional map showing Vp/Vs ratio based on the results of the current study (white circles) and previous RF studies in Ethiopia (red triangles, Hammond

et al. 2011; inverted white triangles, Stuart et al., 2006; magenta pentagon, Dugda et al., 2005), RF in Yemen (white stars, Ahmed et al. 2013).

Table1.

Station	Latitude	Longitude	Elevation (m)	H (km)	Error H (km)	Vp/Vs	Error Vp/Vs	Number of RF
N001	39.3077	13.5545	2148	37.6	2.3	1.73	0.04	46
N002	39.4162	13.5453	2000	38.8	1.9	1.73	0.02	23
N003	39.5007	13.5580	2080	37.6	0.5	1.79	0.02	50
N004	39.5653	13.5775	2265	37.6	0.3	1.73	0.01	67
N005	39.6677	13.6334	2270	38.6	1.6	1.73	0.04	36
N006	39.7805	13.6509	2383	37.0	7.0	1.70	0.10	52
N007	39.8938	13.6922	970	24.2	1.5	1.79	0.05	31
N008	40.0066	13.8406	692	19.4	1.3	1.93	0.02	25
S001	38.9328	11.6591	2904	42.8	1.7	1.79	0.01	27
S003	39.3211	11.8511	3446	41.0	2.0	1.87	0.02	65
S004	39.4903	11.8274	2372	37.2	4.0	1.83	0.06	15
S005	39.5291	11.8387	1931	34.6	1.8	1.75	0.01	56
S006	39.5874	11.8472	2057	34.0	0.4	1.76	0.02	60
S007	39.6583	11.8478	1601	34.0	1.2	1.72	0.03	58
S008	39.7348	11.8621	1491	27.6	1.3	1.85	0.03	52
S009	39.7995	11.8001	1486	28.2	0.5	1.80	0.02	59
S011	39.9164	11.8203	1075	27.6	1.5	1.79	0.01	58
S012	39.9581	11.8717	1007	27.8	1.7	1.79	0.03	20
S013	40.0506	11.8574	914	28.0	2.0	1.79	0.03	27
S014	40.1831	11.8584	827	20.8	1.6	1.95	0.05	38
FINE	40.3100	12.0600	782	21.4	1.7	1.99	0.02	72
S017	40.7044	11.9856	613	23.2	1.5	1.96	0.02	60
S018	40.8044	11.8521	441	21.6	1.0	1.92	0.01	21
S020	40.9667	12.0019	355	19.8	0.6	2.02	0.01	65

Figure 1.

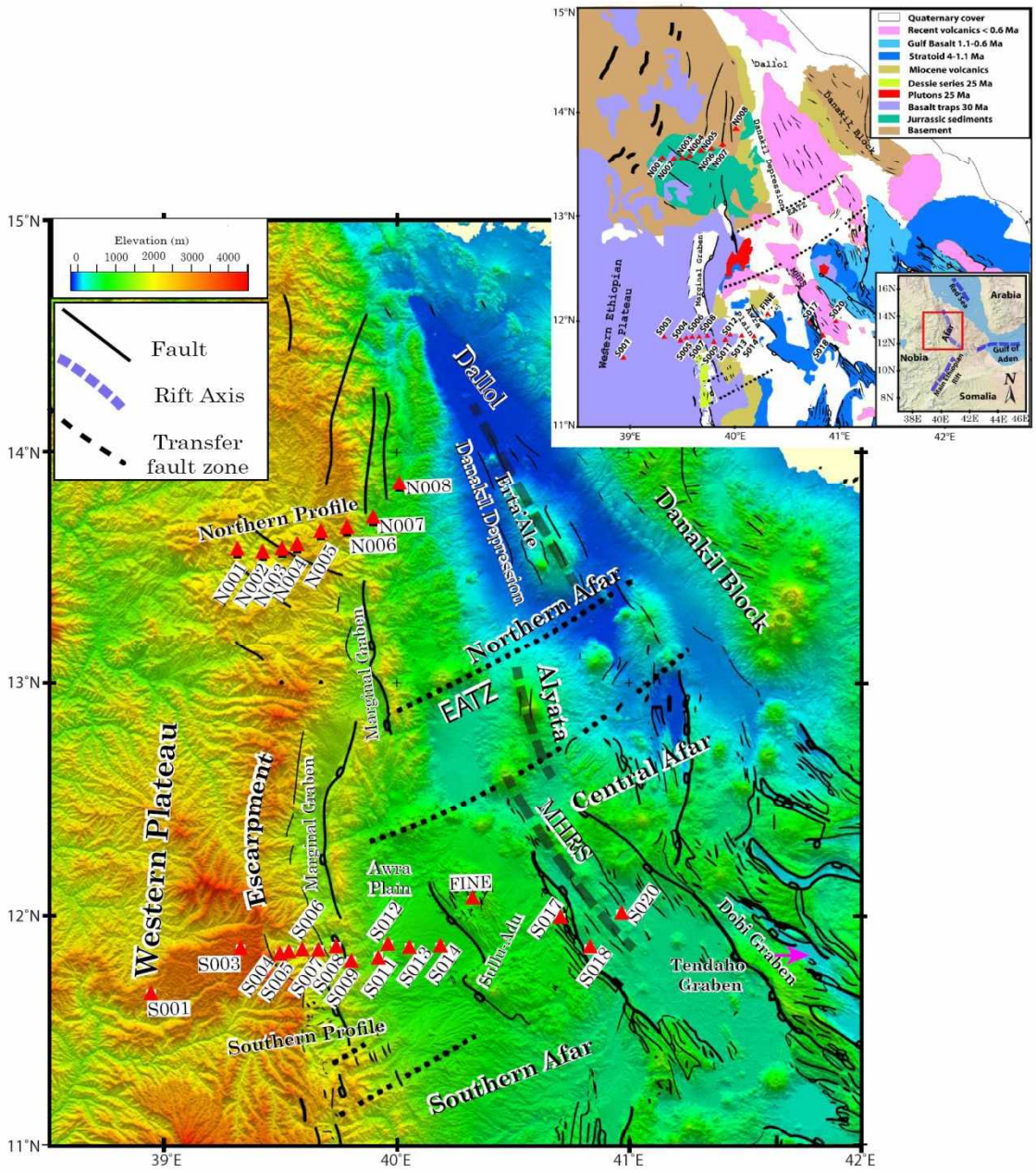
Elevation (m)
0 1000 2000 3000 4000
Fault
Rift Axis
Transfer fault zone
Quaternary cover
Recent volcanics < 0.6 Ma
Gulf Basalt 1.1-0.6 Ma
Stratoid 4-1.1 Ma
Miocene volcanics
Dessie series 25 Ma
Plutons 25 Ma
Basalt traps 30 Ma
Jurrassic sediments
Basement
Dallol
Danakil Block
Danakil Depression
Western Ethiopian Plateau
Marginal Graben
Arabia
Nubia
Somalia
Gulf of Aden
Afar
Northern Profile
Southern Profile
Western Plateau
Escarpment
Marginal Graben
Awra Plain
Tendaho Graben
Dobi Graben
Northern Afar
Central Afar
Southern Afar
EATZ
Alyata
MHRS
Tat'Ale
Sullu-Adu
FINE
N001
N002
N003
N004
N005
N006
N007
N008
S001
S003
S004
S005
S006
S007
S008
S009
S011
S012
S013
S014
S015
S017
S020
15°N
14°N
13°N
12°N
11°N
39°E
40°E
41°E
42°E

Figure 2.

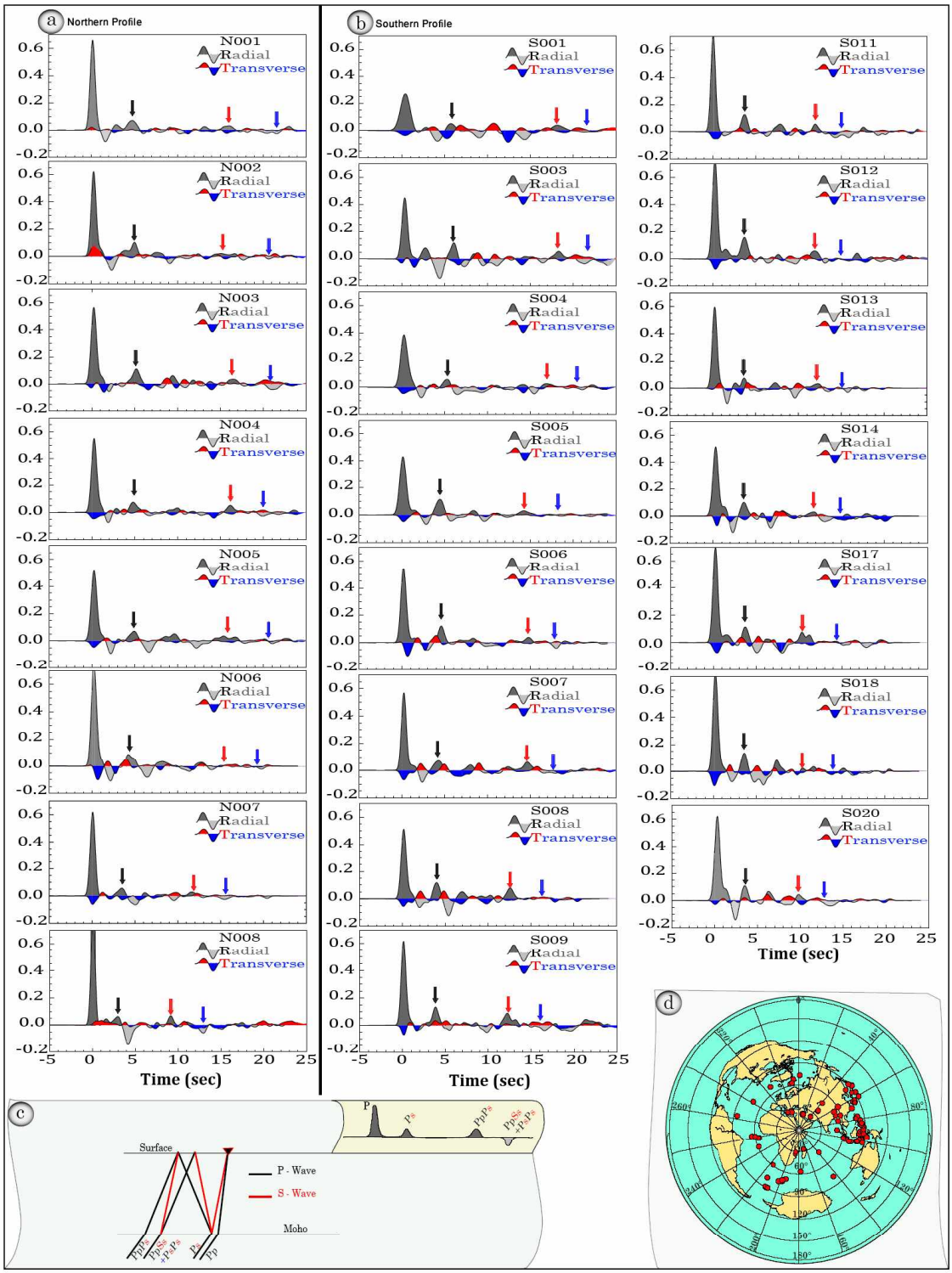
a Northern Profile
b Southern Profile
N001
N002
N003
N004
N005
N006
N007
N008
S001
S003
S004
S005
S006
S007
S008
S009
S011
S012
S013
S014
S017
S018
S020
Radial
Transverse
Time (sec)
c
Surface
P - Wave
S - Wave
Moho
d

Figure 3.

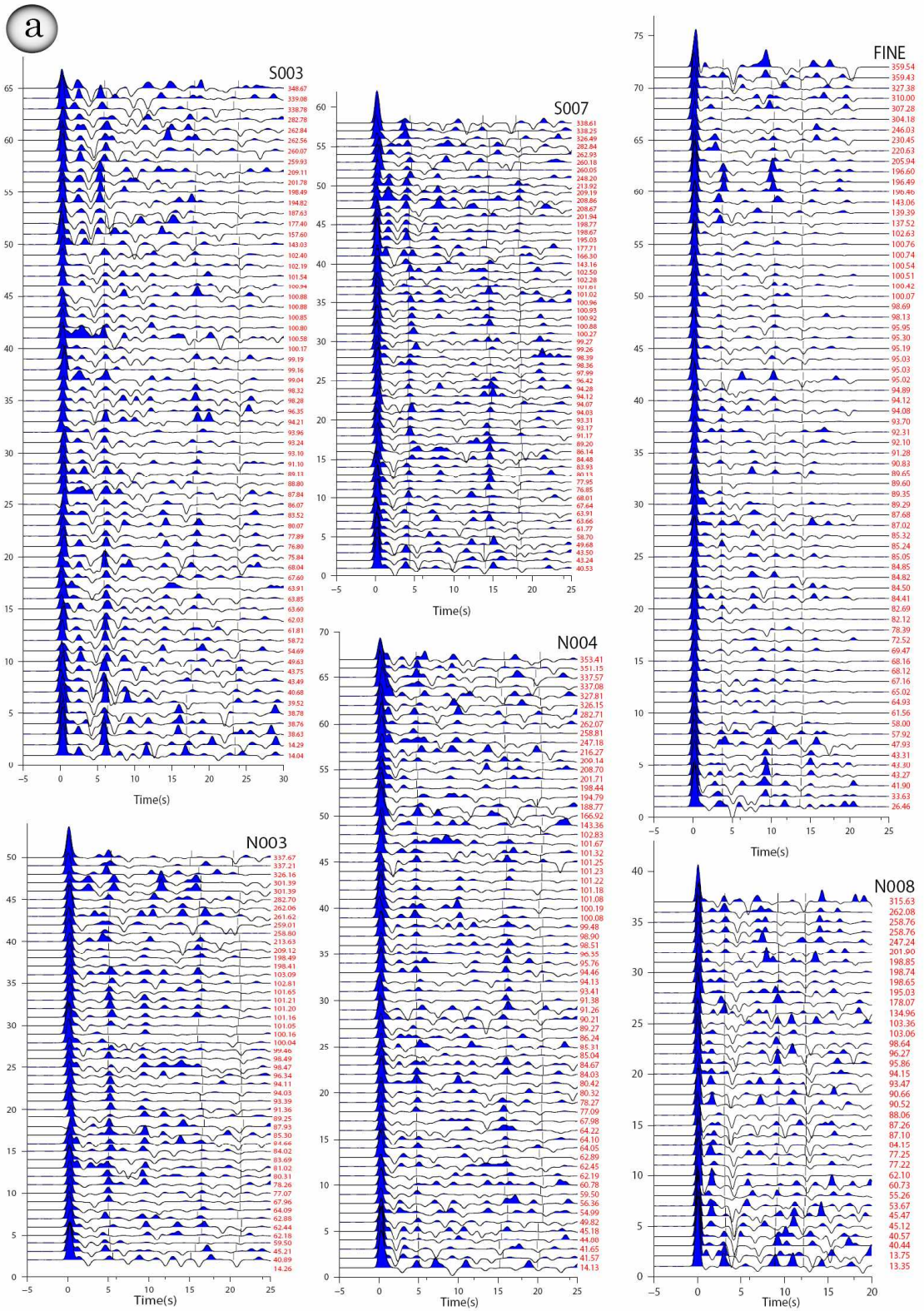

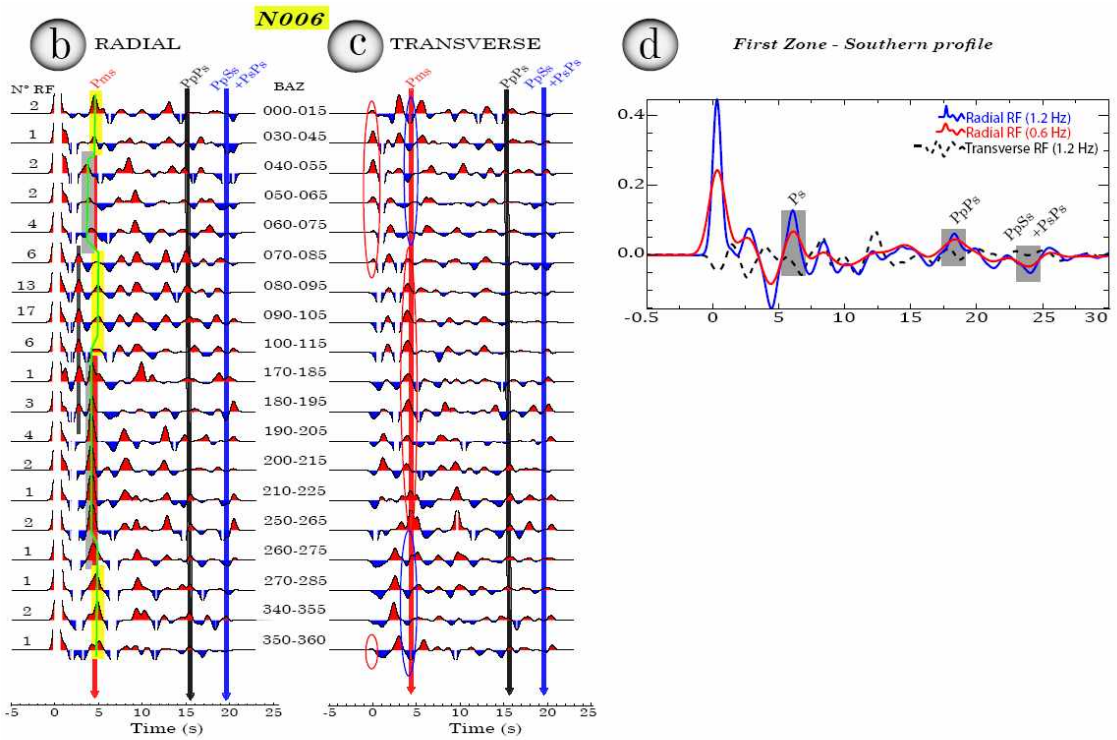
N006
b RADIAL
c TRANSVERSE
d First Zone - Southern profile
N° RF
BAZ
Pms
PpPs
PpSs +PsPs
000-015
030-045
040-055
050-065
060-075
070-085
080-095
090-105
100-115
170-185
180-195
190-205
200-215
210-225
250-265
260-275
270-285
340-355
350-360
Time (s)
Radial RF (1.2 Hz)
Radial RF (0.6 Hz)
Transverse RF (1.2 Hz)
Ps

Figure 4.

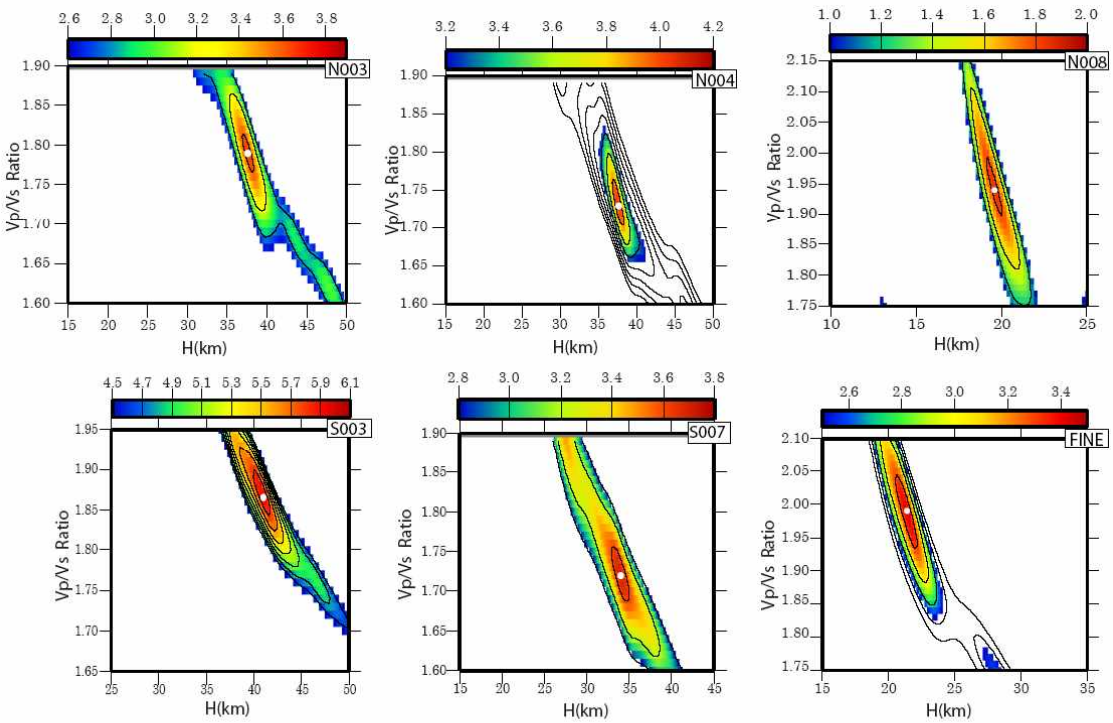
N003
N004
N008
S003
S007
FINE
Vp/Vs Ratio
H(km)

Figure 5.

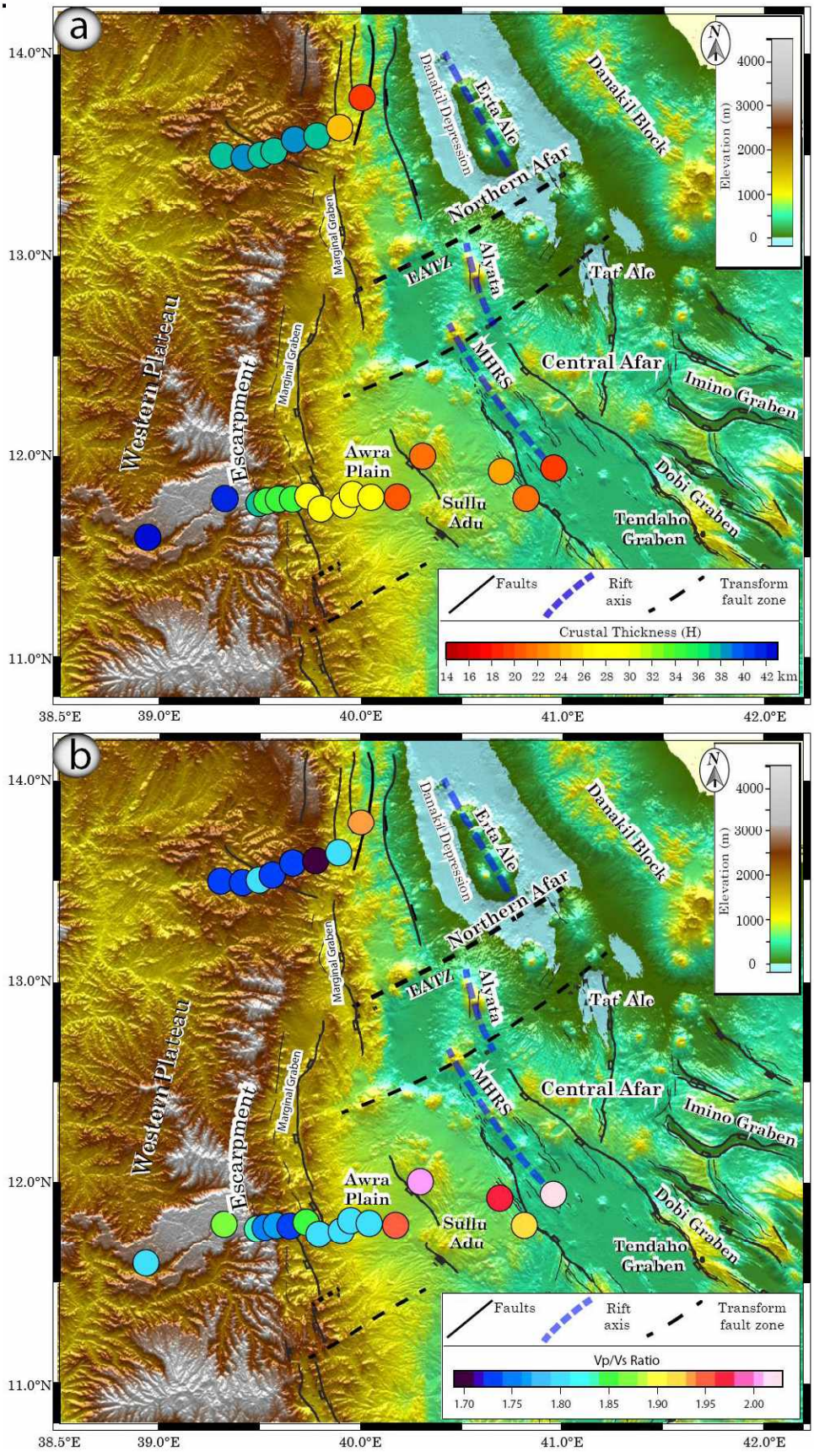
a
b
Danakil Depression
Erta Ale
Danakil Block
Northern Afar
Marginal Graben
EATZ
Alyata
Taf Ale
Western Plateau
Escarpment
MHRS
Central Afar
Imino Graben
Awra Plain
Sullu Adu
Dobi Graben
Tendaho Graben
Elevation (m)
4000
3000
2000
1000
0
N
Faults
Rift axis
Transform fault zone
Crustal Thickness (H)
14 16 18 20 22 24 26 28 30 32 34 36 38 40 42 km
Vp/Vs Ratio
1.70 1.75 1.80 1.85 1.90 1.95 2.00
14.0°N
13.0°N
12.0°N
11.0°N
38.5°E
39.0°E
40.0°E
41.0°E
42.0°E

Figure 6.

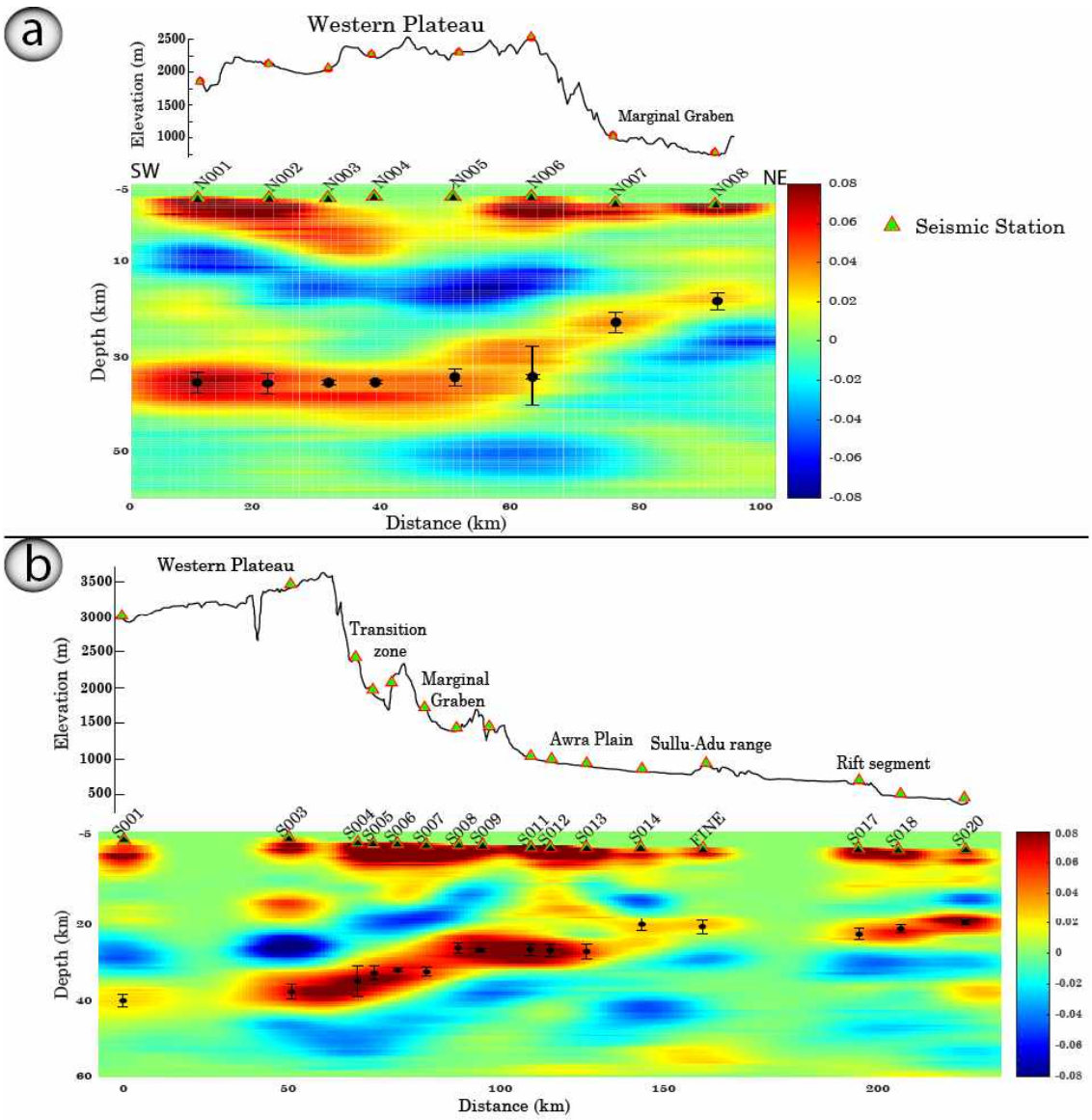
a
Western Plateau
Elevation (m)
2500
2000
1500
1000
Marginal Graben
SW
NE
N001
N002
N003
N004
N005
N006
N007
N008
Seismic Station
Depth (km)
-5
10
30
50
0
20
40
60
80
100
Distance (km)
0.08
0.06
0.04
0.02
0
-0.02
-0.04
-0.06
-0.08
b
Western Plateau
Transition zone
Marginal Graben
Awra Plain
Sullu-Adu range
Rift segment
Elevation (m)
3500
3000
2500
2000
1500
1000
500
S001
S003
S004
S005
S006
S007
S008
S009
S011
S012
S013
S014
FINE
S017
S018
S020
Depth (km)
-5
20
40
60
0
50
100
150
200
Distance (km)
0.08
0.06
0.04
0.02
0
-0.02
-0.04
-0.06
-0.08

Figure 7.

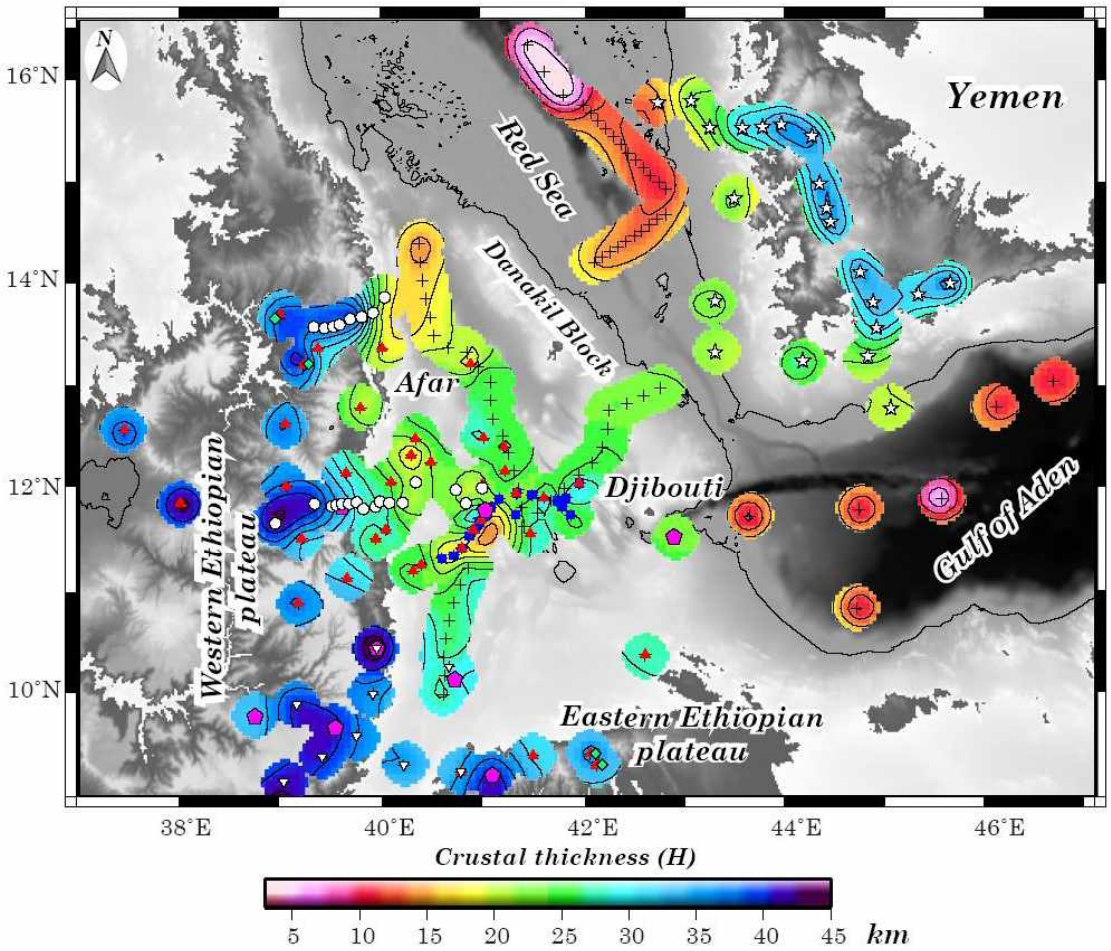
N
16°N
14°N
12°N
10°N
38°E
40°E
42°E
44°E
46°E
Yemen
Red Sea
Danakil Block
Afar
Djibouti
Gulf of Aden
Western Ethiopian plateau
Eastern Ethiopian plateau
Crustal thickness (H)
5
10
15
20
25
30
35
40
45
km

Figure 8.

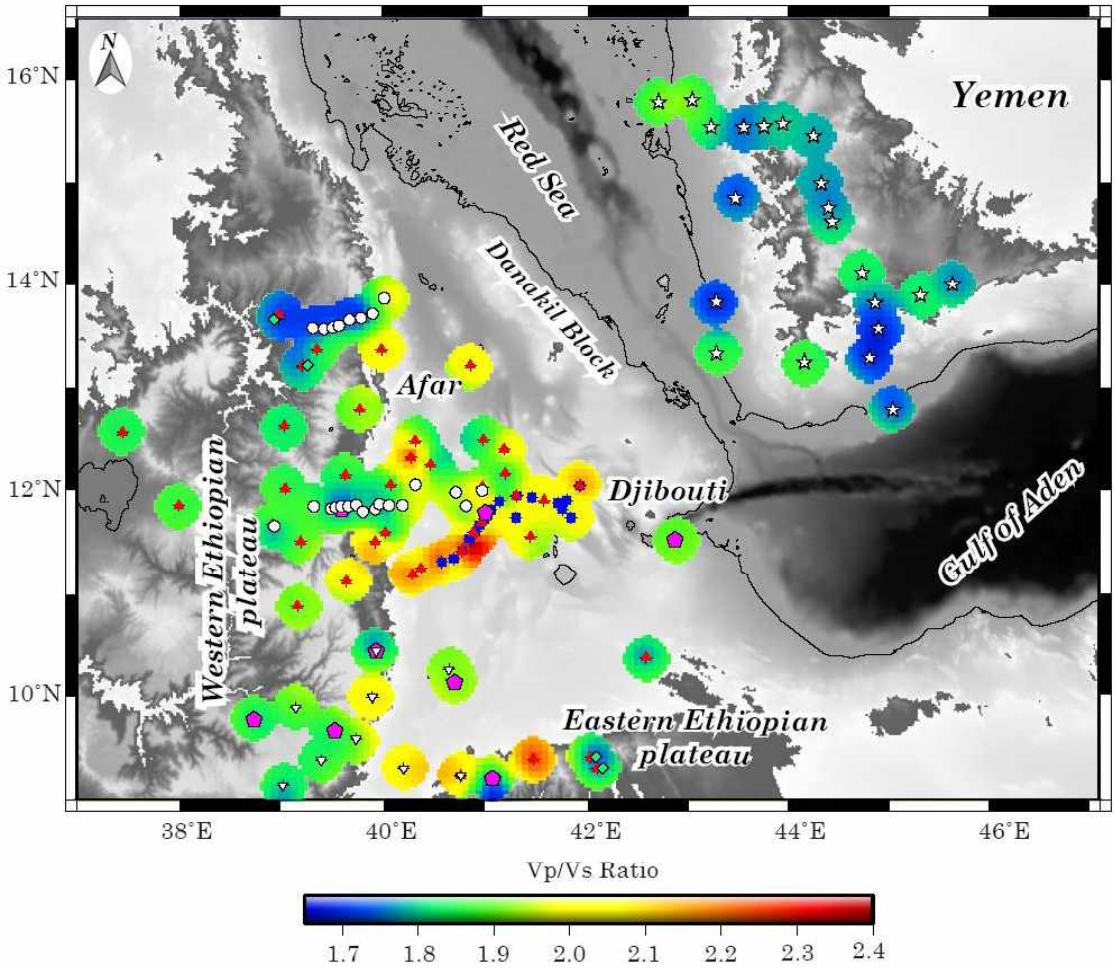
N
16°N
14°N
12°N
10°N
38°E
40°E
42°E
44°E
46°E
Yemen
Red Sea
Danakil Block
Afar
Djibouti
Gulf of Aden
Western Ethiopian plateau
Eastern Ethiopian plateau
Vp/Vs Ratio
1.7
1.8
1.9
2.0
2.1
2.2
2.3
2.4